

Residual distribution schemes for Maxwell's equations

S.S. Neoh, F. Ismail*

School of Aerospace Engineering, Universiti Sains Malaysia, 14300, Malaysia



ARTICLE INFO

Keywords:

Second-order residual distribution
Row-mass-lumping
Time-dependent hyperbolic
Electromagnetic waveguide
Electromagnetic scattering
Electromagnetic radiation

ABSTRACT

This paper aims to deliver another approach of solving hyperbolic system of equation into the field of computational electromagnetics, known as the residual distribution (RD) or fluctuation splitting method. The RD scheme fills the interstice between finite-element method (FEM) and finite-volume method (FVM), where its idea of calculating flux residual imitates the FVM, but the numerical solutions within a discretized triangular mesh is interpolated with similitudes to the FEM. It was originally designed as a remedy to capture shock problem in Euler system under compact stencil, but its extension to linear-preserving scheme which is the main cause of this work, capable of giving second-order-accurate results and is congenial to the FEM framework. The RD scheme is always vertex-centered therefore has all the conserved variables \mathbf{E} and \mathbf{H} located at the same nodal point. This topology evades having both vertex-centered and cell-centered coordination in one single mesh, and permits time-discretization other than the staggered time marching scheme, such as the common backward-time discretization which is unconditionally stable. Another contribution of this work is to suggest that row-mass-lumping of the consistent mass-matrix would not mar too much the second-order-accuracy of LDA-RD scheme, which is an upwind scheme where the mass-matrix an impediment for time-updating during the last decade. A prior reconstruction of the upwind mass-matrix is done before lumping up the mass-matrix so that the time-marching nodal update is consistent with the distribution of mass-matrix. The current work covers 3 basic exercises of electromagnetics, they are 2D radiation problem, 2D scattering problem and 3D waveguide propagation. For the 2D scattering and 3D waveguide problems, the perfect electric conductor (PEC) boundary condition is successfully applied using RD construction.

© 2018 Elsevier Inc. All rights reserved.

1. Introduction

The computational work for electromagnetics was embarked in year 1966 upon the publishing of Yee's algorithm [64]. Originally, the finite-difference time-domain (FDTD) was developed in staggered grid, meaning that the electric and magnetic fields are computed on a set of primary and secondary grids, where the nodes of the secondary grid are placed on the barycenters of the primary mesh. FDTD was then developed in the following decades by a lot of scholars such as Taflove [61] and et cetera. Other field solvers did emerge, like Transmission Line method (TLM) [12,13,25], Finite Element method (FEM) [9,53], or the various Method of Moments (MoM) [9,53]. The most relevant approach to the Residual Distribution method is the Finite-Volume Time-Domain (FVTD), which will be discussed in the next paragraph.

* Corresponding author.

E-mail addresses: nss15_aer003@student.usm.my (S.S. Neoh), aefarzad@usm.my (F. Ismail).

The finite volume method appeared in the community of computational electromagnetics in the very late of 1980s [32,33,54,55], for which can be considered as a numerical solver in-between FDTD and FEM. Finite Volume method has grown its popularity in dealing with conservation laws, because of its high geometrical flexibility and versatility. Instead of discretizing the Maxwell's equations in differential form, FVTD is a conservative method based on the Maxwell's curl equations expressed in their integral form. In general, the FVTD method is based on the characteristic theory [55] and flux-splitting treatment, which separates outgoing (+) and incoming (-) fluxes at each interface between two adjacent cells [10,22], which is similar to its initial design in solving fluid dynamics problems (examples are Euler equations, Navier-Stokes equations). Hermeline [24], Madsen and Ziolkowsky [33] have proposed FVTD method with primary grid and dual cell. Yee, besides his contribution to the FDTD, also attempted to incorporate FVTD method to the FDTD to form some kind of hybrid schemes [65,66]. Finite Volume scheme with the field vectors co-located at the same vertices was being introduced [14,54]. Another second order leap-frog time integration with second-order centered numerical fluxes was developed by Remaki and Piperno [39,43]. The most recent second-order Finite-Volume method is the cell-centered by Ismagilov [28]. Other relevant works in FVTD for electromagnetics could be found in [7,22].

In this work, however, another numerical solver which is very close to Finite-Volume (FV) but slightly different called Residual Distribution (RD) or Fluctuation-Splitting is being proposed for Maxwell's equations. The RD scheme has shown some advantages over FV in their fields of research. Recalling the history of RD method, its pioneer works are claimed to begin from two different research lines [18]. The first line was led by Hall, Morton and their collaborators [52] when they studied cell-vertex FV scheme. Independently, Ni [37] has modified a so-called Lax-Wendroff RD scheme. The second line was started at almost the same time but in different context, when Roe [46] reinterpreted his flux-difference splitting FV scheme, this is where the name fluctuation-splitting enters. The RD method can be viewed as interlinking the FEM with the FV method. The piecewise spatial interpolating function within an elementary cell is similar to the FE method. RD method might provide another option of numerical methods to tackle Maxwell's equations, alongside with FVTD. Both of them can handle unstructured grid, and more importantly, suitable for hyperbolic system of equations because of the upwinding behavior. The RD method for linear Maxwell's equations evades the main difficulty encountered in Euler system, as they do not consist of non-linear fluxes in the quadratic form of the conserved variables. Thus, there is no need of worry for the averaging of conserved variables in the Jacobian fluxes, one of which is the well known Roe-Struijs-Deconinck linearisation [17]. Cell-vertex FV method solves the conservation equation by obtaining the zero flux balance in the normal directions of median dual cell enclosing a particular node with its neighboring nodes. In other words, it is a multiple projection of Riemann problem between the current updating node with all its surrounding nodes. On the other hand, the mechanism of RD method relaxes the flux balance (residual or fluctuation) within each and every elementary cell goes to zero by distributing the remnant of flux balance to the vertices contained within the cell based on the characteristic speed.

This work is much motivated from the way RD scheme serves as an alternative option for FV method in fluid dynamics, in which it resembles FVTD method in certain aspects, but differs in other perspectives. The main objective of present work is to propose an alternative numerical solver to FVTD method in Computational Electromagnetic (CEM). There are two salient advantages of Residual Distribution method. The first of which is the second order spatial convergence of RD scheme under compact stencil. Linear-preserving schemes such as Low Diffusion A (LDA) [59,60] and Lax-Wendroff (LW) achieve second-order-accuracy even with the immediate first layer of adjacent cells being considered for the nodal update, whereby only the first-order upwind FV is obtained under the same compact stencil. The LDA scheme is a truly upwinding scheme and LW is very alike to the FEM Streamline-Upwind Petrov-Galerkin (SUPG), which is a central scheme plus an upwind correction. The only drawback is that both of the above-mentioned RD techniques generate oscillations if the test case contains discontinuity or shock. If that is the case, one would sacrifice the accuracy and use first-order Narrow (N-scheme) [47] instead to suppress the spurious oscillations in the vicinity of the shock. The second advantage is that the RD method is a multidimensional upwinding scheme, that it is less affected by the irregularity of the grid. Similar efforts have been done by Bidégaray and Ghidaglia [8], which performed multidimensional corrections to cell-centered FV methods for Maxwell's equations due to the mesh-dependent structures of the FV solutions. The directional effect of FV method arises from computing fluxes across edges in definite direction.

In fact, there has been works in FVTD electromagnetic which referred to classical works of RD method, and that has thrown some insights to exploit the possibility of RD scheme in CEM. One example is the vertex-centered FVTD in simulating electromagnetic scattering from aerospace configuration [21]. Deore and Chatterjee implemented the cell-vertex based FV method originally proposed by Ni [37] to solve the electromagnetic scattering from NACA0012 airfoil. They also mentioned that Ni's algorithm is a genuinely multidimensional form of the 'fluctuation-signal' approach proposed by Roe [46] in solving time-dependent wave dominating phenomena. Besides that, the RD scheme has been preceded for magnetohydrodynamics (MHD) equations during the beginning of this millennium by Aslan [5], Csik [15], and more recently by Abgrall and his team [4].

The biggest challenge of RD scheme lies within its extension to time-dependent problem. Linear-preserving RD scheme is second-order-accurate in steady state, but Maxwell's equations, which is the main trunk in electrodynamics, do contain time-derivative. The remedy to preserve second-order of accuracy for RD scheme was instigated by Caraeni [11] using mass-matrix. Research group from Polytechnic of di Bari [16,48,50] have attempted substantial ways of constructing the mass-matrix, as long as the distribution of residual is conservative, meaning that no extra fluxes are generated during the numerical simulation. Although the mass-matrix approach makes the distribution of spatial-curl and time-derivative becoming very consistent, it has to be solved implicitly, which is very expensive in term of computational cost. Ricchiuto and

Table 1
Propagating modes of electromagnetic waves.

Mode	Zero field	Propagating field	Fields confined in xy-plane
TE	$E_z = 0$	H_z	E_x, E_y, H_x, H_y
TM	$H_z = 0$	E_z	E_x, E_y, H_x, H_y

Abgrall [44] have suggested another way of high-order mass-lumping to yield an explicit RD scheme for unsteady problem. Another work from Warzyński [63] is by adapting some intermediate Runge-Kutta approximations to be substituted into the mass-matrix, which obviates the excessive use of sub-iterations. Abgrall and his collaborators [3] have developed high-order scheme up to fourth-order accurate in space last year, with iterative formulation still involved for nodal time-stepping. The main objective of this paper is to extend the idea of Residual Distribution scheme to the time-dependent Maxwell equations. Apart from adapting the RD techniques for Maxwell's equations, the authors has also done some improvements over the current RD method for the sake of solving the unsteady hyperbolic system. The contributions from this work can be summarized as following:

1. Introduce an upwind mass-matrix that is consistent with upwind RD scheme. The most salient feature of RD scheme is that it can be pure upwind, which is totally like as one-sided difference formula. Therefore, another alternative way of defining the upwind mass-matrix is provided in this work, which is given in [Section 5.2](#).
2. Performing row-mass-lumping for the consistent upwind mass-matrix. Row-mass-lumping has already been seen in FEM [27,42], but its discussion in RD framework is rather meagre. RD-LW is one example of RD scheme that renders precise numerical results with diagonal lumping of the central mass-matrix. The similar lumping procedure is thus suggested for the spatial-upwind mass-matrix to avoid onerous computation of the mass-matrix. The only option for time-discretization after the row-mass-lumping has taken place is the two-stage Runge-Kutta (RK2) method, which will be given in [Sections 5.3](#) and [5.5](#).

[Section 2](#) of this work lists out the Maxwell's equations, which are the governing equations for this topic. The section after that is on introducing the general properties and basic concepts of RD scheme. [Section 4](#) expatiates on how to discretize the Maxwell's equations such that they can be solved using RD scheme. The first three subsections of [Sections 5.1](#), [5.2](#) and [5.3](#) explain the contributions and alterations made by the authors based on RD framework, and lastly is the [Section 6](#) of results and discussions.

2. The Maxwell's equations

The hyperbolic system, of course with more than one conserved variable, can be expressed in the conservation law for system as follow

$$\frac{\partial \mathbf{U}}{\partial t} + \nabla \cdot \mathcal{F} = 0. \quad (2.1)$$

The time-dependent Maxwell's equations are infallibly a set of hyperbolic system, meaning that they carry the physical significance of electromagnetic waves propagation. The Maxwell's equations comprise of four equations, two for electrostatic or magneto-static, while another two for electrodynamics. In this work, the Maxwell's equations should allude the latter case, which are two coupled equations and are time varying

$$\nabla \times \mathbf{E} = -\mu \frac{\partial \mathbf{H}}{\partial t} \quad (2.2a)$$

$$\nabla \times \mathbf{H} = \mathbf{J} + \epsilon \frac{\partial \mathbf{E}}{\partial t}, \quad (2.2b)$$

where \mathbf{E} is the electric field, \mathbf{H} is the magnetic field, \mathbf{J} is the current density, μ and ϵ being the magnetic permeability and electric permittivity, respectively. In the case devoid of current density, and further assumption that the media is homogeneous such that the permittivity and permeability are constants rather than tensors, the problem could be much simplified.

There are two possible propagation modes for Maxwell's equations, namely the transverse-magnetic (TM) mode and transverse-electric (TE) mode. This comes from the nature of the curl-equations which tells that the magnetic field \mathbf{H} must travel in perpendicular to the electric field \mathbf{E} and vice-versa. If z-direction is the propagating direction, the TE mode has the electric field components confined in the xy-plane while the magnetic field \mathbf{H} is traveling in z-direction, leaving $E_z = 0$. The TM mode works the opposite way round. There are hybrid modes between TE and TM modes in real applications such as optical fibers, but they will not be studied in this work. [Table 1](#) clarifies the field components of each TE and TM mode.

As given in [Table 1](#), E_x, E_y, H_x and H_y do not generally equal to zero. They all have analytical solutions, which are derived from H_z for TE mode (or E_z for TM mode) by differentiation with respect to x and y -coordinates. However, to simplify the problem to two-dimensional case only, one could deliberately decouple a few components, or in other words to set a few

components to zero. For example, in TE mode, one could allow $H_x = 0$ and $H_y = 0$ and the Maxwell's equations (2.2) reduce to

$$\frac{\partial E_x}{\partial t} - \frac{1}{\varepsilon} \left(\frac{\partial H_z}{\partial y} \right) = 0 \quad (2.3a)$$

$$\frac{\partial E_y}{\partial t} - \frac{1}{\varepsilon} \left(-\frac{\partial H_z}{\partial x} \right) = 0 \quad (2.3b)$$

$$\frac{\partial H_z}{\partial t} + \frac{1}{\mu} \left(\frac{\partial E_y}{\partial x} - \frac{\partial E_x}{\partial y} \right) = 0, \quad (2.3c)$$

while for the TM mode, $E_x = 0$ and $E_y = 0$ and the Maxwell's equations (2.2) reduce to

$$\frac{\partial H_x}{\partial t} - \frac{1}{\mu} \left(-\frac{\partial E_z}{\partial y} \right) = 0 \quad (2.4a)$$

$$\frac{\partial H_y}{\partial t} - \frac{1}{\mu} \left(\frac{\partial E_z}{\partial x} \right) = 0 \quad (2.4b)$$

$$\frac{\partial E_z}{\partial t} - \frac{1}{\varepsilon} \left(\frac{\partial H_y}{\partial x} - \frac{\partial H_x}{\partial y} \right) = 0. \quad (2.4c)$$

The Maxwell's equations of (2.3) and (2.4) must be expressed in the form of Eq. (2.1), such as the one given in [8] before one could proceed further to the construction of RD scheme. The Maxwell's equations in two-dimensional are

$$\frac{\partial \mathbf{U}}{\partial t} + \mathcal{A} \cdot \nabla \mathbf{U} = 0, \quad (2.5a)$$

where $\mathcal{A} = (A_x, A_y)$. In TM mode, A_x and A_y are

$$A_x = \begin{pmatrix} 0 & 0 & 0 \\ 0 & 0 & -\frac{1}{\mu} \\ 0 & -\frac{1}{\varepsilon} & 0 \end{pmatrix}, \quad A_y = \begin{pmatrix} 0 & 0 & \frac{1}{\mu} \\ 0 & 0 & 0 \\ \frac{1}{\varepsilon} & 0 & 0 \end{pmatrix}, \quad (2.5b)$$

where $\mathbf{U} = (H_x, H_y, E_z)$.

On the other hand, the characteristic speed vector \mathcal{A} for TE mode is

$$A_x = \begin{pmatrix} 0 & 0 & 0 \\ 0 & 0 & \frac{1}{\varepsilon} \\ 0 & \frac{1}{\mu} & 0 \end{pmatrix}, \quad A_y = \begin{pmatrix} 0 & 0 & -\frac{1}{\varepsilon} \\ 0 & 0 & 0 \\ -\frac{1}{\mu} & 0 & 0 \end{pmatrix}, \quad (2.5c)$$

where $\mathbf{U} = (E_x, E_y, H_z)$.

The full Maxwell's equations for three-dimensional case are $\mathcal{A} = (A_x, A_y, A_z)$

$$A_x = \begin{pmatrix} 0 & 0 & 0 & 0 & 0 & 0 \\ 0 & 0 & 0 & 0 & 0 & \frac{1}{\varepsilon} \\ 0 & 0 & 0 & 0 & -\frac{1}{\varepsilon} & 0 \\ 0 & 0 & 0 & 0 & 0 & 0 \\ 0 & 0 & -\frac{1}{\mu} & 0 & 0 & 0 \\ 0 & \frac{1}{\mu} & 0 & 0 & 0 & 0 \end{pmatrix}$$

$$A_y = \begin{pmatrix} 0 & 0 & 0 & 0 & 0 & -\frac{1}{\varepsilon} \\ 0 & 0 & 0 & 0 & 0 & 0 \\ 0 & 0 & 0 & \frac{1}{\varepsilon} & 0 & 0 \\ 0 & 0 & \frac{1}{\mu} & 0 & 0 & 0 \\ 0 & 0 & 0 & 0 & 0 & 0 \\ -\frac{1}{\mu} & 0 & 0 & 0 & 0 & 0 \end{pmatrix}$$

$$A_z = \begin{pmatrix} 0 & 0 & 0 & 0 & \frac{1}{\varepsilon} & 0 \\ 0 & 0 & 0 & -\frac{1}{\varepsilon} & 0 & 0 \\ 0 & 0 & 0 & 0 & 0 & 0 \\ 0 & -\frac{1}{\mu} & 0 & 0 & 0 & 0 \\ \frac{1}{\mu} & 0 & 0 & 0 & 0 & 0 \\ 0 & 0 & 0 & 0 & 0 & 0 \end{pmatrix} \quad (2.5d)$$

where there all together six conserved variables now, $\mathbf{U} = (E_x, E_y, E_z, H_x, H_y, H_z)$.

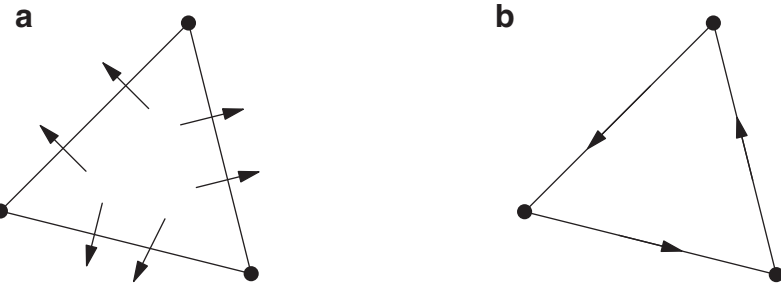


Fig. 1. (a) The volume integration of flux divergence $\iint_T \nabla \cdot \mathcal{F} d\Omega$. (b) The contour integration of flux along the boundary $\int_T \mathcal{F} \cdot d\hat{\ell}$.

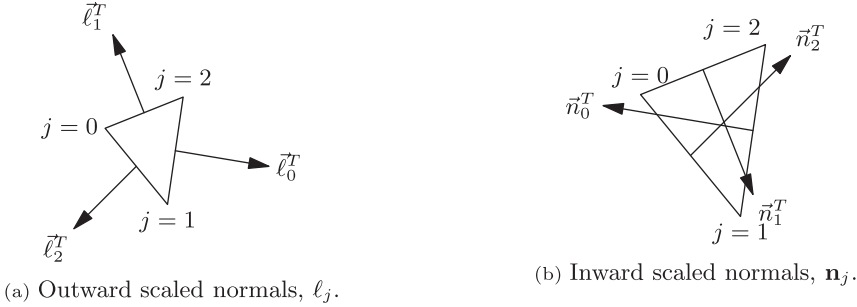


Fig. 2. The scaled edge normals for 2D triangular elements.

3. The fundamentals of residual distribution scheme

Before proceed to the application of RD scheme on electrodynamics problem, it is worth to discuss about the fundamentals of RD method. This section would expound on calculating flux residual and possible ways for distributing it to the local vertices within an element. What follows next is the mathematical construction of RD scheme, which begins from weak formulation, and finally elaborates on several terms relevant to the RD framework. The following discussions on RD scheme are based on the two-dimensional model, with only a small sub-section elaborating on how to obtain a conservative flux residual in three-dimensional model will be given before this section ends. All the properties of RD scheme inherit into the the three-dimensional model indubitably, including the distribution matrix. Their only difference is on the definition of conservative flux residual, which will be discussed therein.

3.1. The concept of residual distribution scheme in two dimensions

The original framework of residual distribution is to undertake Euler equations, dealing mostly with their inviscid advection behavior. In some contexts, Residual Distribution is also referred as Fluctuation-Splitting. The language of ‘residual’ and ‘fluctuation’ bear the same meaning – the flux residual of each primitive element. The working principle of the scheme could be summarized in three steps:

1. Calculate the flux residual within each primitive cell as

$$\Phi^T = \iint_T \nabla \cdot \mathcal{F} d\Omega = \oint_{\partial T} \mathcal{F} \cdot d\hat{\ell}. \quad (3.1)$$

It can be seen that the volume or surface integration can be performed using contour integration by invoking the Green-Gauss theorem. Fig. 1 portrays the two equivalent forms of Green-Gauss theorem. For linear Maxwell’s equations, the volume integration is tantamount to the contour integration. The averaging is not a big issue for linear Maxwell’s equations, but will pose some issues when dealing with Euler system because a non-linear hyperbolic system of equations contains conserved variables \mathbf{U} in its characteristic speed vector \mathcal{A} [1,17,20,38,45]. The over-hat of \mathcal{A} indicates the average value of the characteristic speed within cell T . The contour integration does not incur with the choice of the flux averaging, as the trapezoidal numerical integration along the edges is possible, as depicted in Fig. 2,

$$\oint_{\partial T} \mathcal{F} \cdot d\hat{\ell} = \sum_{j \in T} \left(\frac{\mathcal{F}_{j-1} + \mathcal{F}_{j+1}}{2} \right) \cdot \hat{\ell}_j = \frac{1}{2} \sum_{j \in T} \mathcal{F}_j \cdot \mathbf{n}_j. \quad (3.2)$$

The notation of inward scaled normals, \mathbf{n}_j is commonly adopted in most of the RD contexts. This elaborates clearly why the convention of inwardly scaled normals prevails for the construction of RD scheme.

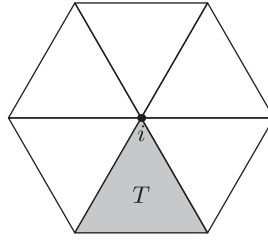


Fig. 3. Set of elements T shared by node i , $T \in \cup \Delta_i$.

2. Calculate the distribution matrix for each vertex, B_j^T .

The RD scheme usually appears as an upwind scheme in CFD works. The distribution matrix B_j^T plays the role of distributing the flux residual Φ^T to downstream vertices according to certain proportion. The category of RD scheme is based upon the multifarious definition of B_j^T .

3. Nodal update by collecting the flux residual Φ^T from elements sharing node i .

The median dual cell enters in the temporal update of RD scheme. For Galerkin's distribution with central-time discretization, an explicit nodal update could be yielded as

$$\mathbf{U}_i^{n+1} = \mathbf{U}_i^n - \frac{\Delta t}{S_i} \sum_{T \in \cup \Delta_i} B_i^T \Phi^T(\mathbf{U}^n), \quad (3.3)$$

where the subscript $T \in \cup \Delta_i$ stands for set of triangular element sharing node i , as shown in Fig. 3. When explicit time-marching scheme is not possible, an implicit solver which is often encountered in RD framework is the pseudo-time iteration.

$$\mathbf{U}_i^{n+1,k+1} = \mathbf{U}_i^{n+1,k} - \frac{\Delta \tau}{S_i} \sum_{T \in \cup \Delta_i} \{\alpha_i^T(\mathbf{U}^{n+1,k}) + B_i^T \Phi^T(\mathbf{U}^{n+1,k})\}, \quad (3.4)$$

where α_i^T contains the time-derivative, usually known as the unsteady residual, k being the fictitious-time counter. This pseudo-time iteration will be mentioned once more in Section 5.4.

3.2. Finite element view of residual distribution scheme

The affinity between Residual Distribution method and Finite-Element method (FEM) is that both of them approximate the solution within a primitive cell using Lagrange interpolating function. The family of Lagrange basis function in use for RD is mostly on linear (P1) element and quadratic (P2) element, although other interpolating functions like Bernstein's has been reported [3]. The formulation of RD scheme starts from either an integral form of Eq. (3.5a)

$$\iint_T \left(\frac{\partial \mathbf{U}}{\partial t} + \nabla \cdot \mathcal{F} \right) d\Omega = 0 \quad \forall T \in \Omega, \quad (3.5a)$$

or a weak form of Eq. (3.5b)

$$\int_0^{+\infty} \iint_{\mathbb{M}^2} \omega_i I \left(\frac{\partial \mathbf{U}}{\partial t} + \nabla \cdot \mathcal{F} \right) d\Omega dt = 0, \quad (3.5b)$$

where ω is a weight function, which appears in the formulation of FE method as well. Similar to the local interpolating function in FE method, the weight ω is compact, meaning that it has some values within a particular triangular cell T , but zero elsewhere. Rossiello and his collaborators [16,50] gave a very detailed account for the formulation of this RD scheme.

In this current paper, only the linear shape function $\psi^T(x, y)$ is considered for each cell. The linear shape function $\psi_i(x, y)$ is equal to unity only at (x_i, y_i) , but zero elsewhere [9] as given in Fig. 4.

The conserved variable \mathbf{U} within a cell is interpolated linearly as shown in Fig. 5a

$$\mathbf{U}_h(x, y, t) = \sum_{j \in T} \mathbf{U}_j(t) \psi_j(x, y), \quad (3.6a)$$

$$\psi_i(x_j, y_j) = \begin{cases} 1 & \text{if } i = j \\ 0 & \text{if } i \neq j \end{cases} \quad (3.6b)$$

Upon the substitution of (3.6a), Eq. (3.5b) becomes

$$\iint_T \omega_i I \left(\frac{\partial \mathbf{U}_h}{\partial t} + \mathcal{A} \cdot \nabla \mathbf{U}_h \right) d\Omega = 0, \quad (3.7)$$

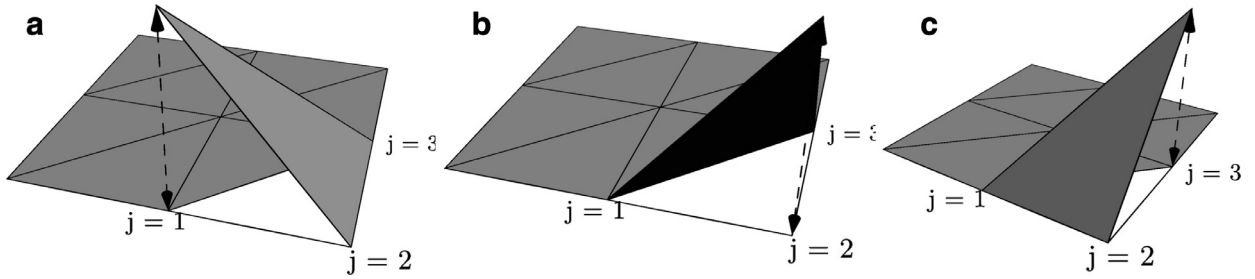


Fig. 4. The Lagrange's type of linear interpolating functions of (a) $\psi_1(x, y)$, (b) $\psi_2(x, y)$ and (c) $\psi_3(x, y)$.

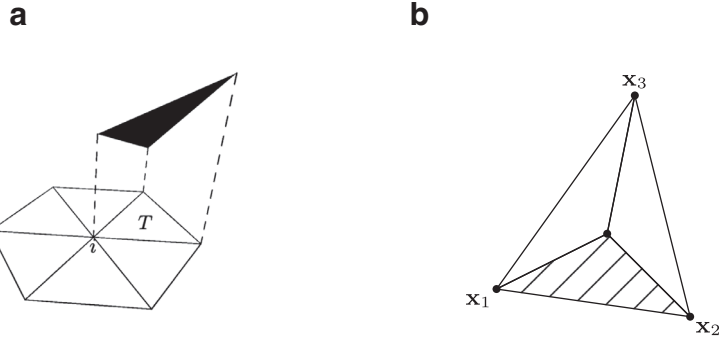


Fig. 5. (a) In RD scheme, conserved variable \mathbf{U} is represented by a linear interpolation function (P1 element). (b) The interpolating function of $\psi_3(\mathbf{x})$ can be represented by simplex coordinate as area function.

with I is the identity matrix of size the number of conserved variables.

Consider the first term of (3.7), which is the time derivative part,

$$\iint_T \omega_i I \frac{\partial \mathbf{U}_h}{\partial t} d\Omega = \sum_{j \in T} \iint_T \omega_i I \psi_j \frac{d\mathbf{U}_j(t)}{dt} d\Omega. \quad (3.8a)$$

Note that $\psi_j(x, y)$ is a spatial interpolating function, thus it does not vary with time. The second term of (3.7), which will be the main concern of this paper, is the flux residual, defined as

$$\begin{aligned} \iint_T \omega_i I \tilde{\mathcal{A}} \cdot \nabla \mathbf{U}_h d\Omega &= \iint_T \omega_i I \sum_{j \in T} \tilde{\mathcal{A}} \cdot \frac{\mathbf{n}_j}{2S_T} \mathbf{U}_j d\Omega \\ &= \sum_{j \in T} \tilde{\mathcal{A}} \cdot \frac{\mathbf{n}_j}{2S_T} \mathbf{U}_j \iint_T \omega_i I d\Omega. \end{aligned} \quad (3.8b)$$

The integral in Eq. (3.8b) is the distribution matrix which will be discussed shortly in next section

$$\iint_T \omega_i I d\Omega = B_i^T. \quad (3.9)$$

Some basic properties of the interpolating function are given in Eq. (3.10). The construction of P1 element allows the gradient of variables \mathbf{U} to be constant within an element T . In this simplex coordinate, for example, the interpolating function for $\psi_j(x, y)$ is determined by the hatched area in Fig. 5b. The rest of the interpolating function follows the same convention. Thus, one arrives at a more compact form for $\psi_1(x, y)$ as

$$\psi_j(x, y) = \frac{1}{2S_T} (\mathbf{x} - \mathbf{x}_{j+1}) \cdot \hat{z} \times (\mathbf{x}_{j-1} - \mathbf{x}_{j+1}), \quad (3.10a)$$

with the sequence of j in the counter-clockwise direction and S_T is the cell area of element T .

$$\nabla \psi_j(x, y) = \frac{\mathbf{n}_j}{2S_T}, \quad (3.10b)$$

where the gradient of the linear interpolating function within a cell is a constant, given as

$$\nabla \mathbf{U}_h = \sum_{j \in T} \nabla \psi_j(x, y) \mathbf{U}_j = \sum_{j \in T} \frac{\mathbf{n}_j}{2S_T} \mathbf{U}_j. \quad (3.10c)$$

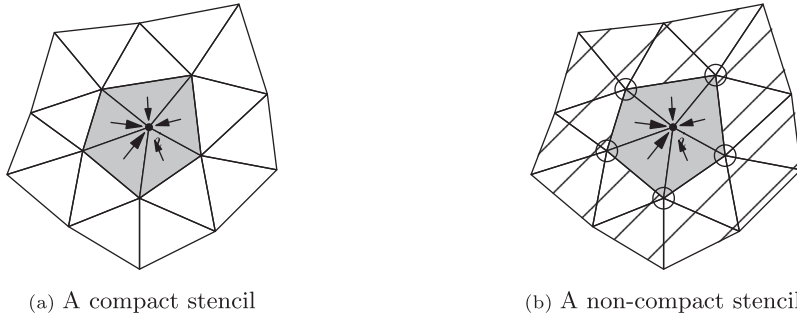


Fig. 6. (a) A compact scheme imbibes only information from its immediate neighboring cells. (b) A non-compact stencil requires data, usually the gradient at all nodes of the surrounding elements.

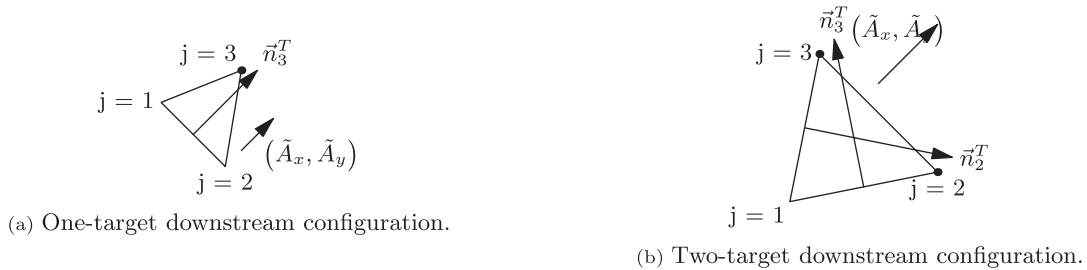


Fig. 7. The one-target and two-target cases meant for RD scheme.

\mathbf{n}_j is the scaled inward normal of the edge opposite to node j , pointing towards the interior of T with the magnitude of that edge length. \hat{z} is the unit vector pointing out of the page, as the area cross product always points in direction perpendicular to the plane. \mathbf{x}_1 , \mathbf{x}_2 and \mathbf{x}_3 are the position vectors for each local vertex and \mathbf{x} is simply just any point within the triangle, since $\psi_j(\mathbf{x})$ is varying with \mathbf{x} locally.

3.3. The basic properties of RD scheme

The main concept of RD scheme is to calculate the flux residual within an elementary cell and after that, distribute the residual accordingly. RD scheme could be classified based on the distribution coefficient β_i^T .

There are several properties of linear RD scheme being investigated over the last three decades, such as its compactness and multidimensional upwinding. There are some other properties of RD scheme which are not mentioned over here but can be found easily in literature [2,18,19,36,51].

3.3.1. Compact stencil

The compactness is one of the innate advantage of RD scheme. This is mainly because of each nodal update collects only flux residual from primitive elements abut on it. This would make parallel computation for large domain less intricate, thus allowing for the construction of a powerful and efficient solver as reported by Mazaheri and Nishikawa [35]. Moreover, a numerical scheme that involves information from its immediate neighbors would require less interpolation from cells further away, hence a less diffusive but still accurate scheme is obtained. Fig. 6 shows the compactness of stencil.

3.3.2. Multidimensional upwind

RD scheme is claimed to evince multidimensional upwinding property. An upwind scheme will distribute the flux residual to downstream nodes, in analogy to the flowing fluid from high potential region to low potential region.

Refer to Eq. (3.8b), the inflow matrix K_i^T is defined as

$$K_j^T = \frac{1}{2} \mathcal{A} \cdot \mathbf{n}_j^T, \quad (3.11)$$

where \mathbf{n}_j^T is the inward pointing normal, as it is the common notation in RD context. In Fig. 7a, the local node $j = 3$ is the only downstream node. On the other hand, Fig. 7b shows an example of two-target downstream configuration as vertices $j = 2, 3$ are the two downstream nodes for element T .

3.3.3. Galerkin's distribution

The discussions of Galerkin's distribution is rather meager in RD scheme, due to the nature of linear advection problem or the hyperbolic system of Euler equations. However, for transient wave equation, the central scheme (or Galerkin scheme)

in space is sometimes proven to be useful. For example, Lax-Wendroff scheme, which is a central scheme in space with a temporal correction for $n + 1/2$ time step, appears to acquit well in most cases where the solutions are smooth and continuous.

3.3.4. Conservative flux residual

Flux residual in RD scheme refers to the integration of the spatial derivative term. Integration over a two-dimension space domain is not that straightforward, especially if the mesh is unstructured. The formulation is getting even more complicated upon extending the idea to three-dimension space domain. Thanks to the Lagrange interpolating function in RD scheme, this obstacle is overcome by two ways.

1. Utilizing the Gauss theorem to convert the integration of the flux divergence term over a control volume to contour integration of the flux along the boundary of each triangular element T . It is averred to be conservative as the trapezoidal integration along the edges of triangle cancels with flux integration from abutted triangle.

$$\Phi^T = \oint_{\partial T} \mathcal{F} \cdot d\hat{\ell} \cong \frac{1}{2} \sum_{j \in T} \mathcal{F}_j \cdot \mathbf{n}_j. \quad (3.12)$$

2. The gradient of the conserved variable is constant within a cell. The gradient is constant in each element under linear reconstruction (P1 element), as alluded by Eqs. (3.8b) and (3.10). Therefore, the area integration of the flux divergence becomes

$$\Phi^T = \iint_T \nabla \cdot \mathcal{F} d\Omega \cong \sum_{j \in T} K_j \mathbf{U}_j. \quad (3.13)$$

This second method will inflict some issues for non-linear hyperbolic system like Euler system, as it contains conserved variables up to quadratic terms. Proper averaging like Roe-Struij-Deconinck linearization [1,17,20] is required since its flux Jacobian contains the conserved variables. Fortunately, the averaging of Jacobian is not needed for Maxwell's equations as they are just linear equations.

Another important feature of the numerical flux residual in (3.12) is its conservation property [51]. Imagine that when one summing up all the flux residual of triangle T in the computational domain Ω , terms which remain are only those on the boundary. This is also called “telescoping property” of the RD flux residual [19,20] as the contributions from all internal edges cancel out

$$\sum_{T \in \Omega} \oint_{\partial T} \mathcal{F} \cdot d\hat{\ell} = \oint_{\partial \Omega} \mathcal{F} \cdot d\hat{\ell}. \quad (3.14)$$

3.3.5. Distribution matrix

After one has determined the local flux residual Φ^T , distribution matrix B_j^T is another critical issue to be dealt with. In general, distribution coefficient indicates the proportion of flux residual to be sent to the downstream nodes (for upwind scheme like LDA)

$$\Phi_j^T = B_j^T \Phi^T. \quad (3.15)$$

The RD scheme is classified based on how the distribution matrix B_j^T is being defined. The two most commonly encountered properties in RD framework are positivity and linearity preservation. Positivity ensures no new extrema in the numerical solution, whereas a scheme that satisfies linearity preservation has a linearly varying solution as long as the distribution matrix B_j^T for any element T is bounded. Example of positive schemes is N-scheme while LDA and Lax-Wendroff schemes are linear-preserving schemes with second-order accuracy. Godunov's theorem ensures that a scheme could not be both positive (or monotone) and linear-preserving at the same time [19]. In order to yield a conservative scheme, the sum of the distribution matrix within a triangular element T should not be larger than unity,

$$\sum_{j \in T} B_j^T = I. \quad (3.16)$$

3.3.6. Linearity preservation

Before entering into the main course of linear-preserving scheme, it is worth mentioning about scalar conservation law as readers might find it more receptive to this idea. The scalar conservation law is

$$\frac{\partial u}{\partial t} + \nabla \cdot \mathbf{F}(u) = 0, \quad (3.17)$$

where

$$\mathbf{F}(u) = u \tilde{\lambda} \Rightarrow \nabla \cdot \mathbf{F} = \tilde{\lambda} \cdot \nabla u. \quad (3.18)$$

The flux residual now is a scalar value, and can be written as

$$\phi^T = \sum_{j \in T} k_j u_j, \quad (3.19)$$

with k_j the inflow parameter

$$k_j = \frac{1}{2} \tilde{\lambda} \cdot \mathbf{n}_j, \quad (3.20)$$

or using the flux contour integration as

$$\phi^T = \frac{1}{2} \sum_{j \in T} \mathbf{F}_j \cdot \mathbf{n}_j. \quad (3.21)$$

Now for scalar conservation law, the distribution coefficient β_j^T is used instead of distribution matrix B_j^T for system. The distribution of flux residual to each vertex relies strongly on the definition of β_j

$$\phi_j^T = \beta_j \phi^T. \quad (3.22)$$

Definition. A RD scheme is said to be linear-preserving if its definition for distribution coefficient β_j^T is bounded [19], such that

$$0 \leq \beta_j^T \leq 1. \quad (3.23)$$

Proposition. The RD scheme for hyperbolic system is linear-preserving if the distribution matrix B_j^T is bounded with

$$0 \leq \det(B_j^T) \leq 1. \quad (3.24)$$

Examples of linear-preserving RD schemes are LDA and LW schemes. Both of them can achieve second-order accuracy in space if P1 element (with linear interpolation within each triangle T) is being employed. Some of the linear-preserving schemes could give numerical results of third-order-accurate by including gradient reconstruction or sub-mesh reconstruction [26,49]. The presumption to maintain the order-of-accuracy is such that the local error of the quadrature integration of flux residual is of order $O(\Delta x^3)$. If the distribution coefficient is bounded, then the accumulated global error would still be preserved at $O(\Delta x^2)$ [18].

$$\Phi^T = O(\Delta x^3) \rightarrow \sum_{T \in \cup \Delta_i} B_i^T \Phi^T = O(\Delta x^2). \quad (3.25)$$

3.3.7. Positivity or monotonicity

Another type of scheme is the positive scheme. A scheme which is positive will produce monotone numerical results by forbidding the generation of new extrema. It usually happened to be the upwind first-order-accurate, but is suitable when handling with problems containing discontinuity or shock. One of the best known positive scheme for RD method is the N-scheme, where N stands for Narrow [56,57]. The definition of distribution matrix B_j^T cannot be pre-defined for N-scheme, therefore it is want to have distributed residual as [19]

$$\Phi_j^N = - \left(\sum_{j \in T} K_j^+ \right)^{-1} K_i^+ \sum_{j \in T} K_j^- (\mathbf{U}_i^n - \mathbf{U}_j^n), \quad (3.26a)$$

or

$$\Phi_j^N = K_i^+ (\mathbf{U}_i - \mathbf{U}_{in}), \quad (3.26b)$$

where the inflow state is

$$\mathbf{U}_{in} = - \left(\sum_{j \in T} K_j^+ \right)^{-1} \sum_{j \in T} K_j^- \mathbf{U}_j. \quad (3.26c)$$

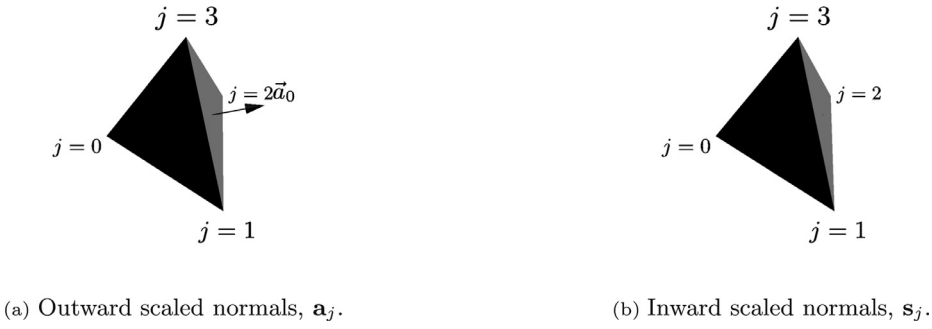
Another alternative for defining the N-scheme is by relating it to the LDA scheme

$$\Phi_j^N = \Phi_j^{LDA} + \mathbf{d}_i^N, \quad (3.27a)$$

where \mathbf{d}_i^N is the local dissipation and \mathbf{U}_{out} the outflow state

$$\mathbf{d}_i^N = K_i^+ (\mathbf{U}_i - \mathbf{U}_{out}), \quad (3.27b)$$

$$\mathbf{U}_{out} = \left(\sum_{j \in T} K_j^+ \right)^{-1} \sum_{j \in T} K_j^+ \mathbf{U}_j. \quad (3.27c)$$

**Fig. 8.** The scaled plane normals for 3D tetrahedral elements.

This second definition of N-Scheme (3.27a), as proposed by Deconinck and Ricchiuto [18], enables the flux residual to be calculated using Eq. (3.12). The telescoping property is then being fulfilled and therefore allowing the N-scheme to be conservative. However, it is very rare to observe shock wave for Maxwell's equations, thus, the positive scheme is not the main concern in this work.

3.3.8. Time step

The final ingredient for the RD scheme is the time-derivative update. In all computations of the following sections, the time-step Δt is calculated such that it fulfills the Courant-Friedrichs-Levy (CFL) condition to ensure the stability of the time update [63]

$$\Delta t = \min_{i \in T_h} \text{CFL} \frac{S_i}{\sum_{T \in \cup \Delta_i} \alpha^T}, \quad (3.28a)$$

where the coefficient α^T is defined as

$$\alpha^T = \frac{1}{2} \max_{j \in T} c \sqrt{S_T}, \quad (3.28b)$$

with $\sqrt{S_T}$ the reference length for element T .

3.4. Residual distribution scheme for three-dimensional problem

The flux residual for three-dimensional problem of

$$\Phi^T = \iiint_T \nabla \cdot \mathcal{F} dV = \iiint_T \mathcal{A} \cdot \nabla \mathbf{U} dV \cong \tilde{\mathcal{A}} \cdot \iiint_T \nabla \mathbf{U} dV,$$

is given by Green-Gauss theorem as

$$\Phi^T = \iiint_T \nabla \cdot \mathcal{F} dV = \oint_{\partial T} \mathcal{F} \cdot \mathbf{d}\mathbf{a}. \quad (3.29)$$

The volume integration is now over the tetrahedral element, and the contour integration now spans over the outward-pointing surface areas that bound the tetrahedral element. This is analogous to the line integral along the boundary in two-dimensional case. Similarly, the trapezoidal rule does applicable to the tetrahedral elements, with \mathbf{a}_j is the area vector pointing outward and \mathbf{s}_j is the inward pointing normal with the magnitude of the surface area, as shown in Fig. 8.

The trapezoidal rule approximates the flux \mathcal{F} that penetrates plane \mathbf{s}_j to be the average flux value of its three vertices.

$$\Phi^T = \oint_{\partial T} \mathcal{F} \cdot \mathbf{d}\ell = \sum_{j \in T} \left(\frac{\mathcal{F}_{j+1} + \mathcal{F}_{j+2} + \mathcal{F}_{j+3}}{3} \right) \cdot \mathbf{a}_j = \frac{1}{3} \sum_{j \in T} \mathcal{F}_j \cdot \mathbf{s}_j. \quad (3.30)$$

Switching to three-dimensional case, the barycentric or simplex coordinate would give a very similar form of

$$\Psi_j = \frac{V_j}{V_T}, \quad (3.31a)$$

$$\nabla \Psi_j = \frac{1}{3V_T} \mathbf{s}_j, \quad (3.31b)$$

where \mathbf{s}_j is the inward area vector of the plane opposite to node j . With these minor alterations, the unsteady and flux residuals could be attain, respectively as

$$\iiint_T \omega_i I \frac{\partial \mathbf{U}_h}{\partial t} dV = \sum_{j \in T} \frac{d\mathbf{U}_j}{dt} \iiint_T \omega_i I \psi_j dV, \quad (3.32a)$$

$$\iiint_T \omega_i I \mathcal{A} \cdot \nabla \mathbf{U}_h dV = \sum_{j \in T} \frac{\tilde{\mathcal{A}} \cdot \mathbf{s}_j}{3V_T} \mathbf{U}_j \iiint_T \omega_i I dV. \quad (3.32b)$$

With this finite-element notation of RD scheme, the inflow matrix for three-dimensional problem is expressed as

$$K_j^T = \frac{1}{3} \tilde{\mathcal{A}} \cdot \mathbf{s}_j, \quad (3.33)$$

and the equivalence of Eq. (3.13) in 3D becomes

$$\Phi^T = \iiint_T \nabla \cdot \mathcal{F} dV \cong \sum_{j \in T} K_j \mathbf{U}_j. \quad (3.34)$$

In general, all the basic properties of RD scheme in two-dimensional case are applicable to three-dimensional situation.

4. Discretization of Maxwell's equations

Unlike Euler system in fluid dynamics, Maxwell's equations comprise set of linear equations (for the simplest case, as non-linear Maxwell's equations do exist in more advanced context). This would make the implementation of RD scheme on Maxwell's equations becomes less complicated.

This section begins by extending the RD scheme to system of equations, and after that the formulations of three different RD schemes will be presented with some brief explanations attached to it. The conservative flux residual in two-dimensional case is given in Eqs. (3.12) and (3.13), and inflow matrix is as stated in (3.11). The counterpart of flux residual in three-dimensional problem is defined in Eqs. (3.30) and (3.34), where (3.33) is the three-dimensional inflow matrix. From now onwards, these several definitions will be referred whenever flux residual Φ^T is encountered.

4.1. Steger-Warming decomposition

The hyperbolic system of equations always have real eigenvalues, thus making the diagonalization of the equations become plausible. Steger and Warming [58] have demonstrated on splitting the Euler system for fluid dynamics according to the characteristics, with the eigenvalues being the speed of sound. Cell-centered or vertex-centered FV is no longer new in computational electromagnetics, and the Steger-Warming decomposition has been applied to Maxwell's equations in constructing the upwind FV scheme [8,22]. It is rather oblivious that for linear Maxwell's equations, with \mathcal{A} independent of \mathbf{U} , is written as Eq. (2.5a) and \mathcal{A} is just equivalent to the Jacobian of fluxes in Euler system, $\partial \mathcal{F} / \partial \mathbf{U}$. The next thing is to construct the inflow matrix of the RD scheme, K_j

$$K_j = \frac{1}{2} \mathcal{A} \cdot \mathbf{n}_j,$$

where \mathbf{n}_j is the scaled inward pointing normal of the edge opposite to vertex j , with $|\mathbf{n}_j|$ its magnitude whereas η_{jx} and η_{jy} are its corresponding unit normals, such that

$$\mathbf{n}_j = \eta_{jx} |\mathbf{n}_j| \mathbf{i} + \eta_{jy} |\mathbf{n}_j| \mathbf{j}.$$

The eigenvalues of the inflow matrix K_j are $\pm c$ and 0, where $c = 1/\sqrt{\mu\epsilon}$ is the speed of light in the medium. Likewise to the Jacobian matrix of FV, the flux-splitting for K_j is possible, with the same notations that R stands for a set of right-eigenvectors and Λ is the diagonal matrix

$$K_j = \frac{|\mathbf{n}_j|}{2} R \Lambda R^{-1}, \quad (4.1a)$$

with eigenvalues λ in their ascending order along its diagonal components [8],

$$\Lambda = \begin{bmatrix} -c & 0 & 0 \\ 0 & 0 & 0 \\ 0 & 0 & c \end{bmatrix}. \quad (4.1b)$$

Z is the intrinsic impedance of a medium $Z = \sqrt{\mu/\epsilon}$. By using the components of equations, the flux-splitting allows the inflow matrix K_j to be split into the "directional" matrices [8], so called the positive inflow matrix K_j^+ and negative inflow matrix K_j^- ,

$$K_j^\pm = \frac{|\mathbf{n}_j|}{2} R \Lambda^\pm R^{-1}, \quad (4.1c)$$

and the absolute inflow matrix $|K_j|$ as

$$|K_j| = \frac{|\mathbf{n}_j|}{2} R |\Lambda| R^{-1}. \quad (4.1d)$$

Therefore, the inflow matrix of Maxwell's equations can be written as

$$K_j = K_j^+ + K_j^-; \quad K_j^\pm = \frac{1}{2} (K_j \pm |K_j|). \quad (4.2)$$

The inflow matrices for *TM mode* in two-dimensional case are:

$$K_j = \frac{|\mathbf{n}_j|}{2} \begin{bmatrix} 0 & 0 & \eta_{jy}/\mu \\ 0 & 0 & -\eta_{jx}/\mu \\ \eta_{jy}/\varepsilon & -\eta_{jx}/\varepsilon & 0 \end{bmatrix}, \quad (4.3a)$$

$$K_j^\pm = \frac{|\mathbf{n}_j|}{4} \begin{bmatrix} \pm c\eta_{jy}^2 & \mp c\eta_{jx}\eta_{jy} & c\eta_{jy}/Z \\ \mp c\eta_{jx}\eta_{jy} & \pm c\eta_{jx}^2 & -c\eta_{jx}/Z \\ c\eta_{jy}Z & -c\eta_{jx}Z & \pm c \end{bmatrix}, \quad (4.3b)$$

$$|K_j| = \frac{|\mathbf{n}_j|}{2} \begin{bmatrix} c\eta_{jy}^2 & -c\eta_{jx}\eta_{jy} & 0 \\ -c\eta_{jx}\eta_{jy} & c\eta_{jx}^2 & 0 \\ 0 & 0 & c \end{bmatrix}, \quad (4.3c)$$

where $\mathbf{U} = (H_x, H_y, E_z)$.

The inflow matrices for *TE mode* in two-dimensional case are:

$$K_j = \frac{|\mathbf{n}_j|}{2} \begin{bmatrix} 0 & 0 & -\eta_{jy}/\varepsilon \\ 0 & 0 & \eta_{jx}/\varepsilon \\ -\eta_{jy}/\mu & \eta_{jx}/\mu & 0 \end{bmatrix}, \quad (4.4a)$$

$$K_j^\pm = \frac{|\mathbf{n}_j|}{4} \begin{bmatrix} \pm c\eta_{jy}^2 & \mp c\eta_{jx}\eta_{jy} & -c\eta_{jy}Z \\ \mp c\eta_{jx}\eta_{jy} & \pm c\eta_{jx}^2 & c\eta_{jx}Z \\ -c\eta_{jy}/Z & c\eta_{jx}/Z & \pm c \end{bmatrix}, \quad (4.4b)$$

$$|K_j| = \frac{|\mathbf{n}_j|}{2} \begin{bmatrix} c\eta_{jy}^2 & -c\eta_{jx}\eta_{jy} & 0 \\ -c\eta_{jx}\eta_{jy} & c\eta_{jx}^2 & 0 \\ 0 & 0 & c \end{bmatrix}, \quad (4.4c)$$

where $\mathbf{U} = (E_x, E_y, H_z)$.

The inflow matrices for *three-dimensional* case are:

$$K_j = \frac{1}{3} \mathbf{s}_j \cdot \mathbf{s}_j = \frac{1}{3} \begin{bmatrix} 0 & 0 & 0 & 0 & s_{jz}/\varepsilon & -s_{jy}/\varepsilon \\ 0 & 0 & 0 & -s_{jz}/\varepsilon & 0 & s_{jx}/\varepsilon \\ 0 & 0 & 0 & s_{jy}/\varepsilon & -s_{jx}/\varepsilon & 0 \\ 0 & -s_{jz}/\mu & s_{jy}/\mu & 0 & 0 & 0 \\ s_{jz}/\mu & 0 & -s_{jx}/\mu & 0 & 0 & 0 \\ -s_{jy}/\mu & s_{jx}/\mu & 0 & 0 & 0 & 0 \end{bmatrix}. \quad (4.5a)$$

The positive inflow matrix is

$$\begin{aligned} K_j^+ &= \frac{1}{3} R \Lambda^+ R^{-1} \\ &= \frac{1}{6} \begin{bmatrix} (s_{jy}^2 + s_{jz}^2)c & -s_{jx}s_{jy}c & -s_{jx}s_{jz}c & 0 & s_{jz}Zc & -s_{jy}Zc \\ -s_{jx}s_{jy}c & (s_{jx}^2 + s_{jz}^2)c & -s_{jy}s_{jz}c & -s_{jz}Zc & 0 & s_{jx}Zc \\ -s_{jx}s_{jz}c & -s_{jy}s_{jz}c & (s_{jx}^2 + s_{jy}^2)c & s_{jy}Zc & -s_{jx}Zc & 0 \\ 0 & -s_{jz}/Zc & s_{jy}/Zc & (s_{jy}^2 + s_{jz}^2)c & -s_{jx}s_{jy}c & -s_{jx}s_{jz}c \\ s_{jz}/Zc & 0 & -s_{jx}/Zc & -s_{jx}s_{jy}c & (s_{jx}^2 + s_{jz}^2)c & -s_{jy}s_{jz}c \\ -s_{jy}/Zc & s_{jx}/Zc & 0 & -s_{jx}s_{jz}c & -s_{jy}s_{jz}c & (s_{jx}^2 + s_{jy}^2)c \end{bmatrix}, \quad (4.5b) \end{aligned}$$

where $\mathbf{s}_j = s_{jx}\mathbf{i} + s_{jy}\mathbf{j} + s_{jz}\hat{\mathbf{k}}$ is the scaled normal vector opposite to vertex j . $\mathbf{U} = (E_x, E_y, E_z, H_x, H_y, H_z)$ is the set of conserved variables. Since the complete Maxwell's equations in 3D comprise of a 6×6 matrix, there are six eigenvalues, in ascending order of $-c, -c, 0, 0, +c, +c$.

4.2. Lax-Wendroff RD scheme (RD-LW)

Lax-Wendroff scheme does not only have its fame for the finite-difference method, but has also been one of the pioneer work in the development of RD scheme. It was very orthodox in the research field of RD as the only explicit time-updating

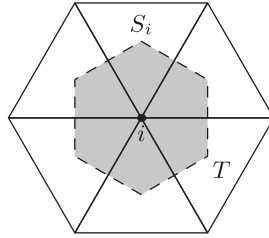


Fig. 9. The hatched region is the median dual cell S_i , and T is the primitive triangular element.

scheme that gives second-order-accuracy for time-dependent problem without introducing the mass-matrix [48,49], not until very lately that another flux-difference approach in RD framework by Ismail and Chizari [29] which vouches to give second-order-accurate with explicit time-update. This is because of the Galerkin's weight function occupied in the weak formulation of the LW scheme which allows mass-lumping and yet does not deteriorate the spatial order of accuracy. Rossiello and his collaborators [48–50] have provided some very clear derivations of LW in two-dimensional RD framework, which would only be summarized herein. The LW scheme could be derived from the integral form (by letting $\omega_i = 1$) as

$$\iint_{S_i} \left(\frac{\partial \mathbf{U}_h}{\partial t} + \nabla \cdot \mathcal{F}_h(\mathbf{U}) \right)^{n+\frac{1}{2}} d\Omega = 0, \quad (4.6)$$

where S_i is the median dual cell encompasses node i as shown in Fig. 9. Essentially, the LW scheme is a two-level time-discretization at t^n and t^{n+1} , with the spatial flux residual evaluated at $t^{n+1/2}$. By invoking the Taylor expansion series of time derivative at $t^{n+1/2}$, and equating them to the spatial flux residual, which is the second term in Eq. (4.6),

$$\begin{aligned} (\nabla \cdot \mathcal{F}_h)^{n+\frac{1}{2}} &= - \left(\frac{\partial \mathbf{U}_h}{\partial t} \right)^{n+\frac{1}{2}} \\ &= - \left(\frac{\partial \mathbf{U}_h}{\partial t} \right)^n - \frac{\Delta t}{2} \left(\frac{\partial^2 \mathbf{U}_h}{\partial t^2} \right)^n + O(\Delta t^2) \\ &= (\nabla \cdot \mathcal{F}_h)^n + \frac{\Delta t}{2} \tilde{\mathcal{A}} \cdot \nabla \left(\frac{\partial \mathbf{U}_h}{\partial t} \right)^n + O(\Delta t^2), \end{aligned} \quad (4.7)$$

having used the relation $\partial/\partial t = -\tilde{\mathcal{A}} \cdot \nabla$. The time derivative is to be discretized using forward Euler time step

$$\left(\frac{d \mathbf{U}_i}{dt} \right)^{n+\frac{1}{2}} = \frac{\mathbf{U}_i^{n+1} - \mathbf{U}_i^n}{\Delta t} + O(\Delta t^2). \quad (4.8)$$

and the full details of the derivation will be omitted to prevent from interminable discussions upon it, as they could be readily found in [18,48].

The time-marching scheme is usually performed in explicit nodal update, so that the RD-LW approach in *two-dimensional* case is

$$\mathbf{U}_i^{n+1} = \mathbf{U}_i^n - \frac{\Delta t}{S_i} \sum_{T \in \cup \Delta_i} \left[\frac{1}{3} I + \frac{\Delta t}{2S_T} K_i^T \right] \Phi_j^T(\mathbf{U}^n). \quad (4.9a)$$

It is a *central* scheme with a temporal correction term, with distribution coefficient reads

$$B_j^{LW} = \frac{I}{3} + \frac{\Delta t}{2S_T} K_j^T, \quad (4.9b)$$

with Δt the time step after discretizing the time derivative term, and I is the identity matrix.

Likewise for the *three-dimensional* situation, the explicit nodal update of RD-LW reads

$$\mathbf{U}_i^{n+1} = \mathbf{U}_i^n - \frac{\Delta t}{V_i} \sum_{T \in \cup \Delta_i} \left[\frac{1}{4} I + \frac{\Delta t}{2V_T} K_i^T \right] \Phi_j^T(\mathbf{U}^n). \quad (4.10)$$

The term in the parenthesis would be the distribution matrix B_i^T .

4.3. Galerkin's distribution

Galerkin approach is seldom encountered in RD framework, as it dealt mostly with linear advection or Euler system, which is hyperbolic. The pure spatial Galerkin's distribution for steady Euler system is untenable, unless with some artificial dissipations. The LW scheme could work for steady Euler problem, with the $(\Delta t/2S_T)K_i^T$ functioning as the streamline dissipation, which ends up in the close form to the Streamline-Upwind Petrov-Galerkin (SUPG) Finite-Element method.

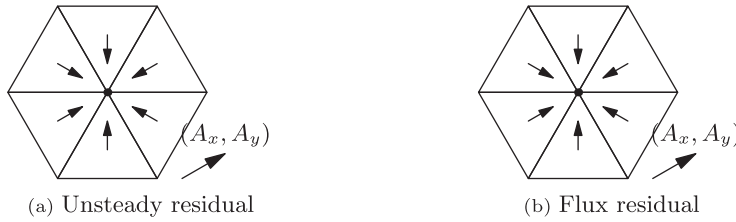


Fig. 10. The distribution of residuals for Galerkin-RD scheme in 2D case. Both the unsteady residual α_i^T and the flux residual Φ^T are distributed equally to all the vertices.

For Maxwell's equations, however, they are time-dependent and the spatial Galerkin approach is feasible, ensuing from the success of LW scheme and some of the central scheme in CEM [22,24]. Starting from the weak formulation for node i ,

$$\sum_{T \in \cup \Delta_i} \iint_T \psi_i I \left(\frac{\partial \mathbf{U}_h}{\partial t} + \nabla \cdot \mathcal{F}_h \right) d\Omega = 0, \quad (4.11)$$

The general form of Galerkin-RD scheme is then be given as

$$\sum_{T \in \cup \Delta_i} (\alpha_i^T + B_i^T \Phi^T) = 0 \quad (4.12)$$

For *two-dimensional* model, the flux residual is the same as already been mentioned in [Section 3](#),

$$B_j^T = \frac{I}{3}. \quad (4.13a)$$

The consistent mass-matrix, such as the one appears in FEM could be obtained as

$$\alpha_i^T = \sum_{j \in T} M_{ij}^T \frac{d\mathbf{U}_j}{dt}, \quad (4.13b)$$

with

$$M_{ij}^T = S_T \frac{I}{12} \begin{bmatrix} 2 & 1 & 1 \\ 1 & 2 & 1 \\ 1 & 1 & 2 \end{bmatrix}. \quad (4.13c)$$

On the other hand, the *three-dimensional* case is almost the same, except for the distribution matrix B_j^T

$$B_j^T = \frac{I}{4}, \quad (4.14)$$

and the equivalent mass-matrix in *three dimension* reads

$$M_{ij}^T = S_T \frac{I}{20} \begin{bmatrix} 2 & 1 & 1 & 1 \\ 1 & 2 & 1 & 1 \\ 1 & 1 & 2 & 1 \\ 1 & 1 & 1 & 2 \end{bmatrix}. \quad (4.15)$$

[Fig. 10](#) envisages the Galerkin-RD scheme in some geometrical sketches.

4.4. Low diffusion A (LDA) - Flux residual

The LDA scheme is capable of giving second-order-accuracy in space, that is when taking the flux residual Φ^T alone, without considering the time derivative. Consider the weak formulation of the time-dependent system of equations,

$$\sum_{T \in \cup \Delta_i} \iint_T \omega_i I \left(\frac{\partial \mathbf{U}_h}{\partial t} + \nabla \cdot \mathcal{F}_h(\mathbf{U}) \right) d\Omega \cong 0. \quad (4.16)$$

If the weight function ω_i is equal to the Lagrange interpolating function ψ_i , then the scheme is called Galerkin scheme as in FE framework. If $\omega_i \neq \psi_i$, the scheme is known as Petrov-Galerkin approach. Definitely, LDA scheme is not a Galerkin method as the choice of the weight function ω_i must abide with the property

$$\frac{I}{S_T} \iint_T \omega_j d\Omega = B_j^T, \quad (4.17)$$

where B_j^T is the distribution matrix.

The spatial flux residual could be then obtained as

$$\begin{aligned} \iint_T \omega_i I (\mathcal{A}_h \cdot \nabla \mathbf{U}_i) d\Omega &= (\tilde{\mathcal{A}} \cdot \nabla \mathbf{U}_i) \iint_T \omega_i I d\Omega \\ &= B_i^T \Phi^T. \end{aligned} \quad (4.18a)$$

Similarly, the manipulation of the time-derivative term, hereafter called as the unsteady residual,

$$\begin{aligned} \iint_T \omega_i I \sum_{j \in T} \psi_j^T \frac{d\mathbf{U}_j}{dt} d\Omega &= \sum_{j \in T} \frac{d\mathbf{U}_j}{dt} \iint_T \omega_i I \psi_j^T d\Omega \\ &= \sum_{j \in T} M_{ij}^T \frac{d\mathbf{U}_j}{dt}, \end{aligned} \quad (4.18b)$$

where

$$M_{ij}^T = \iint_T \omega_i I \psi_j^T d\Omega. \quad (4.18c)$$

For hyperbolic system, the extension leads to matrix operation

$$B_j^T = K_j^+ \left(\sum_{j \in T} K_j^+ \right)^{-1}, \quad (4.19)$$

where $K_j^+ = R \Lambda^+ R^{-1}$ is defined in Eq. (4.1c).

The discretized RD-LDA scheme for both *two-dimensional* and *three-dimensional* cases are given as following:

$$\sum_{T \in \cup \Delta_i} \left[\sum_{j \in T} M_{ij}^T \left(\frac{d\mathbf{U}}{dt} \right)_j + B_i^T \Phi^T \right] = 0, \quad (4.20)$$

with the definition of distribution matrix as given in Eq. (4.19). The general form of the upwind mass-matrix is not presented here, but in Section 5.2.

5. Modifications of RD schemes for Maxwell's equations

The first two subsections of Sections 5.1 and 5.2 will expatiate on contributions made by the authors. The order-of-accuracy analysis will be given first to emphasize on the consistency between distributing flux residual and unsteady residual. The concept of Section 5.3 is borrowed from FEM framework for the RD-LDA scheme. With the aid of two-stage Runge-Kutta (RK2) time-updating procedure, the RD-LDA scheme could be made explicit. The time-discretization and pseudo-time are nothing new, but is detained here until all the other discussions are finished since they involve some knowledge from Sections 5.2 and 5.3.

5.1. Order-of-accuracy for RD discretization

RD scheme and FV method share the same discretizing concept, that is both methods solve the hyperbolic system in integral form. All the RD schemes discussed in this work are linear-preserving scheme, meaning that they are capable of preserving the second-order-accuracy. Some of the similar proofs can be found from [18,50]. Starting from the weak formulation of the governing equation in computational domain $\Omega \subseteq \{(x, y) : \mathbb{R}^2\}$,

$$\begin{aligned} &\iint_{\Omega} \omega_i I \left(\frac{\partial \mathbf{U}_h}{\partial t} + \tilde{\mathcal{A}} \cdot \nabla \mathbf{U} \right) dx dy \\ &= \sum_{T \in \Omega} \iint_T \omega_i I \left(\frac{\partial \mathbf{U}_h}{\partial t} + \tilde{\mathcal{A}} \cdot \nabla \mathbf{U} \right) dx dy \\ &\cong \sum_{T \in \cup \Delta_i} \left\{ \iint_T \omega_i I \sum_{j \in T} \psi_j \frac{d\mathbf{U}_j}{dt} dx dy + \iint_T \omega_i I \tilde{\mathcal{A}} \cdot \nabla \mathbf{U}_j dx dy \right\} \text{ deduction 1} \\ &= \sum_{T \in \cup \Delta_i} \left\{ \sum_{j \in T} \iint_T \omega_i I \psi_j dx dy \frac{d\mathbf{U}_j}{dt} + \sum_{j \in T} \tilde{\mathcal{A}} \cdot \nabla \mathbf{U}_j \iint_T \omega_i I dx dy \right\} \text{ deduction 2} \\ &= \sum_{T \in \cup \Delta_i} \left\{ \sum_{j \in T} M_{ij}^T \frac{d\mathbf{U}_j}{dt} + B_i^T \sum_{j \in T} K_j \mathbf{U}_j \right\} \end{aligned} \quad (5.1)$$

Deduction 1: The weight function ω_i is compact, so that the summation of all triangular cells in domain Ω ($T \in \Omega$) reduces to set of elements sharing node i ($T \in \cup \Delta_i$).

Deduction 2: The Jacobian \mathcal{A} and gradient of conserved variables for linear interpolating function (P1 element) are constant within each element, and therefore the integration of flux divergence term over any triangular cell does not vary.

To understand the local truncation errors, the easiest way is to use the Taylor expansion series in both time and space at $\mathbf{U}(x_i, y_i, t^n)$. The symbolic notations in the Taylor expansion series that follows are as given in Fig. 3. The leapfrog time-discretization is used to demonstrate the influence of second-order-accurate time-discretization. The two-stage Runge-Kutta method, which will be discussed shortly, works in a quite similar way to the leapfrog time-discretization, except that the flux residual has to be evaluated at $t^{n+1/2}$ instead of t^n . Say j is the immediate neighbours of node i with some displacements from it,

$$\frac{d\mathbf{U}_j^n}{dt} = \frac{\mathbf{U}_j^{n+1} - \mathbf{U}_j^{n-1}}{2\Delta t} + O(\Delta t^3). \quad (5.2)$$

The backward time-discretization will preserve second-order of accuracy in a much similar way. First of all, \mathbf{U}_j^{n+1} and \mathbf{U}_j^{n-1} have to be expanded from \mathbf{U}_i^n as

$$\begin{aligned} \mathbf{U}_j^{n+1} &= \underbrace{\mathbf{U}_i^n}_{1} + \left(\underbrace{\Delta t \frac{\partial \mathbf{U}_i^n}{\partial t}}_{2} + \underbrace{\Delta x_{ij} \frac{\partial \mathbf{U}_i^n}{\partial x}}_{3} + \underbrace{\Delta y_{ij} \frac{\partial \mathbf{U}_i^n}{\partial y}}_{4} \right) \\ &\quad + \frac{1}{2} \left(\underbrace{\frac{\partial^2 \mathbf{U}_i^n}{\partial t^2} \Delta t^2}_{5} + \underbrace{\frac{\partial^2 \mathbf{U}_i^n}{\partial x^2} \Delta x_{ij}^2}_{6} + \underbrace{\frac{\partial^2 \mathbf{U}_i^n}{\partial y^2} \Delta y_{ij}^2}_{7} + \underbrace{2\Delta t \Delta x_{ij} \frac{\partial^2 \mathbf{U}_i^n}{\partial t \partial x}}_{8} + \underbrace{2\Delta x_{ij} \Delta y_{ij} \frac{\partial^2 \mathbf{U}_i^n}{\partial x \partial y}}_{9} + \underbrace{2\Delta t \Delta y_{ij} \frac{\partial^2 \mathbf{U}_i^n}{\partial t \partial y}}_{10} \right) \\ &\quad + O(h^3). \end{aligned} \quad (5.3a)$$

$$\begin{aligned} \mathbf{U}_j^{n-1} &= \underbrace{\mathbf{U}_i^n}_{1} + \left(\underbrace{-\Delta t \frac{\partial \mathbf{U}_i^n}{\partial t}}_{2} + \underbrace{\Delta x_{ij} \frac{\partial \mathbf{U}_i^n}{\partial x}}_{3} + \underbrace{\Delta y_{ij} \frac{\partial \mathbf{U}_i^n}{\partial y}}_{4} \right) \\ &\quad + \frac{1}{2} \left(\underbrace{\frac{\partial^2 \mathbf{U}_i^n}{\partial t^2} \Delta t^2}_{5} + \underbrace{\frac{\partial^2 \mathbf{U}_i^n}{\partial x^2} \Delta x_{ij}^2}_{6} + \underbrace{\frac{\partial^2 \mathbf{U}_i^n}{\partial y^2} \Delta y_{ij}^2}_{7} - \underbrace{2\Delta t \Delta x_{ij} \frac{\partial^2 \mathbf{U}_i^n}{\partial t \partial x}}_{8} + \underbrace{2\Delta x_{ij} \Delta y_{ij} \frac{\partial^2 \mathbf{U}_i^n}{\partial x \partial y}}_{9} - \underbrace{2\Delta t \Delta y_{ij} \frac{\partial^2 \mathbf{U}_i^n}{\partial t \partial y}}_{10} \right) \\ &\quad + O(h^3). \end{aligned} \quad (5.3b)$$

Likewise, for the purely spatial Taylor expansion series of \mathbf{U}_j at time level t^n ,

$$\begin{aligned} \mathbf{U}_j^n &= \underbrace{\mathbf{U}_i^n}_{11} + \left(\underbrace{\Delta x_{ij} \frac{\partial \mathbf{U}_i^n}{\partial x}}_{12} + \underbrace{\Delta y_{ij} \frac{\partial \mathbf{U}_i^n}{\partial y}}_{13} \right) \\ &\quad + \frac{1}{2} \left(\underbrace{\frac{\partial^2 \mathbf{U}_i^n}{\partial x^2} \Delta x_{ij}^2}_{14} + \underbrace{\frac{\partial^2 \mathbf{U}_i^n}{\partial y^2} \Delta y_{ij}^2}_{15} + \underbrace{2\Delta x_{ij} \Delta y_{ij} \frac{\partial^2 \mathbf{U}_i^n}{\partial x \partial y}}_{16} \right) + O(h^3). \end{aligned} \quad (5.3c)$$

For the approximation of time derivative using Eq. (5.2), one has to subtract Eq. (5.3b) from Eq. (5.3a). Take note that terms 1, 3, 4, 6, 7 and 9 are eliminated for any proper time-discretization, even if the time-integration formula is just first-order-accurate. Since the second-order time-discretization is being used, then term-5 will not be there as well. Thus, one yields

$$\frac{d\mathbf{U}_j^n}{dt} = \left(\underbrace{\frac{\partial \mathbf{U}_i^n}{\partial t}}_{2} \right) + \left(\underbrace{\Delta x_{ij} \frac{\partial^2 \mathbf{U}_i^n}{\partial t \partial x}}_{8} + \underbrace{\Delta y_{ij} \frac{\partial^2 \mathbf{U}_i^n}{\partial t \partial y}}_{10} \right) + O(h^2). \quad (5.4a)$$

The spatial flux residual is obtained by multiplying the inflow matrix on Eq. (5.3c) to give

$$K_j \mathbf{U}_j^n = K_j \left[\underbrace{\mathbf{U}_i^n}_{11} + \left(\underbrace{\Delta x_{ij} \frac{\partial \mathbf{U}_i^n}{\partial x}}_{12} + \underbrace{\Delta y_{ij} \frac{\partial \mathbf{U}_i^n}{\partial y}}_{13} \right) + \frac{1}{2} \left(\underbrace{\frac{\partial^2 \mathbf{U}_i^n}{\partial x^2} \Delta x_{ij}^2}_{14} + \underbrace{\frac{\partial^2 \mathbf{U}_i^n}{\partial y^2} \Delta y_{ij}^2}_{15} + \underbrace{2 \Delta x_{ij} \Delta y_{ij} \frac{\partial^2 \mathbf{U}_i^n}{\partial x \partial y}}_{16} \right) + O(h^3) \right]. \quad (5.4b)$$

where Δt is the time step, Δx_{ij} and Δy_{ij} are the displacement vectors of vertex j from node i . The summation of $j \in T$ from all immediate elements $T \in \cup \Delta_i$ over Eq. (5.4b) will obviate term-11. Summing Eqs. (5.4a) and (5.4b) over set of triangles sharing node i will give

$$\sum_{T \in \cup \Delta_i} \sum_{j \in T} M_{ij}^T \frac{d\mathbf{U}_j^n}{dt} = \sum_{T \in \cup \Delta_i} \sum_{j \in T} M_{ij}^T \left[\underbrace{\frac{\partial \mathbf{U}_i^n}{\partial t}}_2 + \left(\underbrace{\Delta x_{ij} \frac{\partial^2 \mathbf{U}_i^n}{\partial t \partial x}}_8 + \underbrace{\Delta y_{ij} \frac{\partial^2 \mathbf{U}_i^n}{\partial t \partial y}}_{10} \right) + O(h^2) \right], \quad (5.5a)$$

$$\begin{aligned} \sum_{T \in \cup \Delta_i} B_i^T \sum_{j \in T} K_j \mathbf{U}_j^n &= \sum_{T \in \cup \Delta_i} B_i^T \sum_{j \in T} K_j \left[\left(\underbrace{\Delta x_{ij} \frac{\partial \mathbf{U}_i^n}{\partial x}}_{12} + \underbrace{\Delta y_{ij} \frac{\partial \mathbf{U}_i^n}{\partial y}}_{13} \right) \right. \\ &\quad \left. + \frac{1}{2} \left(\underbrace{\frac{\partial^2 \mathbf{U}_i^n}{\partial x^2} \Delta x_{ij}^2}_{14} + \underbrace{\frac{\partial^2 \mathbf{U}_i^n}{\partial y^2} \Delta y_{ij}^2}_{15} + \underbrace{2 \Delta x_{ij} \Delta y_{ij} \frac{\partial^2 \mathbf{U}_i^n}{\partial x \partial y}}_{16} \right) + O(h^3) \right]. \end{aligned} \quad (5.5b)$$

Term-8 and term-10 in Eq. (5.5a) are of order $O(h)$ while term-14, term-15 and term-16 in Eq. (5.5b) are of the order $O(h^2)$, and they will not cancel away completely for the second-order RD schemes. The key thing to preserve the second-order-accuracy of the RD scheme is that terms-2, 12 and 13 must be removed after recollecting the terms from the governing equation

$$\frac{\partial \mathbf{U}_i^n}{\partial t} + \frac{\partial \mathbf{U}_i^n}{\partial x} + \frac{\partial \mathbf{U}_i^n}{\partial y} = 0. \quad (5.6)$$

This would rely strongly on the choice of M_{ij}^T , and those examples given in Appendix A comply with the condition that

$$\sum_{j \in T} M_{ij}^T = S_T B_i^T, \quad (5.7)$$

provided that the scheme is conservative under Eq. (3.16). It becomes clear by now that Eq. (5.1) is

$$\sum_{T \in \cup \Delta_i} \left\{ \sum_{j \in T} M_{ij}^T \frac{d\mathbf{U}_j^n}{dt} + B_i^T \sum_{j \in T} K_j \mathbf{U}_j^n \right\} = O(h^3). \quad (5.8)$$

Since $M_{ij}^T = O(h^2)$ is an integration over cell area, thus the summation in Eq. (5.5a) is of $O(h^3)$.

The symbol h represents the small intervals of time or space for they are almost of the same magnitude if CFL condition is being fulfilled (3.28a).

The local truncation error is $O(h^3)$, and if the distribution matrix is bounded, then the global truncation error is of $O(h^2)$, where the second-order-accuracy is preserved.

$$\begin{aligned} TE(\mathbf{U}_h) : &= \sum_{i \in \Omega} \sum_{T \in \cup \Delta_i} \left\{ \sum_{j \in T} M_{ij}^T \frac{d\mathbf{U}_j^n}{dt} + B_i^T \sum_{j \in T} K_j \mathbf{U}_j^n \right\} \\ &= O(h^2) \end{aligned} \quad (5.9)$$

5.2. Upwind mass-matrix for LDA scheme

The handling of unsteady residual α_i^T is crucial to preserve the second-order-accuracy of the LDA scheme in time-dependent problem. There are several ways of getting the consistent mass-matrix for RD-LDA scheme, including the one



Fig. 11. The LDA scheme in 2D scene. The unsteady residual α_i^T is distributed in an upwind manner alike to the flux residual Φ^T , based on the definition of distribution matrix B_j^T .

that follows exactly the streamline-upwind Petrov-Galerkin (SUPG) in FEM [34]. The discussion of currently available consistent mass-matrix is given in [Appendix A](#) as the main objective here should emphasize on the alterations made by the authors.

Two-dimension.

The general form of the weight function ω_i is seldom presented in RD framework, and is always assumed to be the SUPG weight function

$$\omega_i I = \left(I\psi_i + B_i^T - \frac{I}{3} \right). \quad (5.10)$$

In this work, however, a third possible way of constructing the mass-matrix is suggested by re-defining the weight function as

$$\omega_i I = 3B_i^T \psi_i. \quad (5.11a)$$

By using this definition of weight function, the consistent-upwind mass-matrix is in a much simpler form of

$$M_{ij}^T = \frac{S_T}{4} \begin{bmatrix} 2B_1^T & B_1^T & B_1^T \\ B_2^T & 2B_2^T & B_2^T \\ B_3^T & B_3^T & 2B_3^T \end{bmatrix}, \quad (5.11b)$$

with $B_j^T = I/3$ for Galerkin's and $B_j^T = K_j^+ [\sum_{j \in T} K_j^+]^{-1}$ for LDA's. The row-mass-lumping gives only diagonal components,

$$M_{ij}^T = \begin{cases} S_T B_j^T, & i = j \\ 0, & i \neq j \end{cases} \quad (5.12)$$

The row-mass-lumping behaves to maintain the second-order-accuracy in space, although with some degrees of depreciation compared to the scheme without undergoing mass-lumping.

Proposition. If RD scheme in steady state is second-order-accurate if B_j^T is bounded, then, distributing both the flux residual and unsteady residual under the same definition of B_j^T will still give a second-order-accurate scheme.

The preservation of second-order-accuracy for RD scheme in steady problem

$$\sum_{T \in \cup \Delta_i} B_i^T \Phi^T = 0 \longrightarrow TE(\mathbf{U}_h) := O(h^2), \quad (5.13)$$

will imply second-order-accuracy for time-dependent problem in a much similar manner

$$\sum_{T \in \cup \Delta_i} B_i^T \left[S_T \frac{d\mathbf{U}_i}{dt} + \Phi^T \right] = 0 \longrightarrow TE(\mathbf{U}_h) := O(h^2). \quad (5.14)$$

Corollary. If B_j^T is bounded, then $S_T B_j^T$ is also bounded

$$0 \leq \det(B_j^T) \leq 1 \implies 0 \leq \det(S_T B_j^T) \leq 1. \quad (5.15)$$

provided that the mesh is small such that S_T is always smaller than unity.

This upwind weight function might fit the LDA scheme better, as it has no distribution to the upstream vertices, as shown in [Fig. 12b](#). [Fig. 11](#) shows how the unsteady residual has to be distributed consistently with the spatial flux residual in LDA-RD scheme.

5.3. Row-mass-lumping in RD schemes

When tackling unsteady problem, the explicit time-marching scheme for LDA scheme would probably fail to preserve the order of accuracy, if an improper explicitly lumped update scheme is used, regardless the order of multistage Runge-Kutta for time update [48]. This has beset the RD community over the past, with several papers published to grapple with this difficulty.

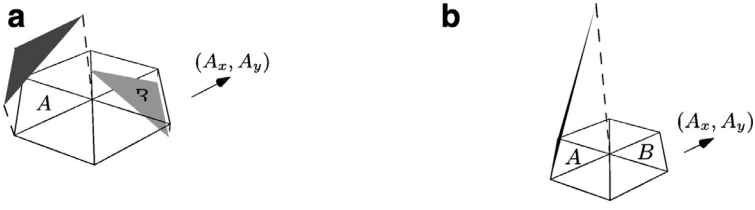


Fig. 12. The weight function for different definition of weight function, (a) represents Petrov-Galerkin weight function of Eq. (5.10) and (b) is the sketch-out for Eq. (5.11a).

The mass-lumping technique is originally appeared in Finite-Element framework [27,42]. Over the decades, mass-lumping is suspected to be culpable for the loss of order-of-accuracy. Therefore, when dealing with time-dependent problem, the CFD community have several approaches other than the mass-lumping. The most straightforward way would be solving the discretized RD scheme implicitly [16], but these sub-iterations within iterations is very time consuming. Another way proposed by [44] is by adapting high-order mass-lumping, such that the lumping could appear in two forms, one is selectively-lumped while another one is globally-lumped. This method gives explicit time-marching scheme, but the amount of mathematics involved requires scrupulous implementation of the code. Warzyński and et al [63] devised their explicit scheme by putting a two-stage Runge-Kutta time-update, where an intermediate guess for the next time step is often computed before its value is used for the mass-matrix calculation to obtain a more polished result. The more recent flux-vector splitting approach by Ismail and his collaborator [29] gives a clear-cut explicit RD scheme without much concerning about the consistency between steady and unsteady residuals.

In this work, however the row-mass-lumping is adapted into the RD schemes, as an alternative to solving an overloaded mass-matrix. The motivation of this comes from the fact that if the LW scheme could be updated explicitly with a promising high accuracy, what about the performance of lumped upwind RD-LDA scheme or the lumped RD-Galerkin scheme, since the LW is in fact made explicit under proper mass-lumping [50]. The derivation of LW scheme from weak formulation perspective shows the conspicuous need of row-mass-lumping in order to get an explicit LW scheme. The summary from [50] will be attached in Appendix B for reference. To be more assured about the mass-lumping effect on unsteady discretization based on Eqs. (5.5a) and (5.5b), one would still get rid of term-2, term-12 and term-13, at least for some structured grids.

After the row-mass-lumping of (5.11b), the discretized RD-Galerkin scheme and RD-LDA scheme give RD-Galerkin (2D).

$$S_i \frac{d\mathbf{U}_i}{dt} + \sum_{T \in \cup \Delta_i} \frac{l}{3} \Phi_T = 0, \quad (5.16a)$$

RD-Galerkin (3D).

$$V_i \frac{d\mathbf{U}_i}{dt} + \sum_{T \in \cup \Delta_i} \frac{l}{4} \Phi_T = 0, \quad (5.16b)$$

RD-LDA (2D).

$$\sum_{T \in \cup \Delta_i} \left[B_i^T S_T \frac{d\mathbf{U}_i}{dt} + B_i^T \Phi_T \right] = 0, \quad (5.16c)$$

RD-LDA (3D).

$$\sum_{T \in \cup \Delta_i} \left[B_i^T V_T \frac{d\mathbf{U}_i}{dt} + B_i^T \Phi_T \right] = 0. \quad (5.16d)$$

An explicit nodal update could be obtained for Galerkin-RD scheme and RD-LDA scheme in proviso that no backward-time discretization is used.

5.4. Pseudo-time stepping

When the backward-time discretization is being used, the RD scheme can no longer be solved explicitly, but some time-implicit mechanism has to be involved. In FV and RD frameworks, Eq. (5.17) is very popular to drive an equation to its approximate solution, the pseudo-time delta $\Delta\tau$ is iterated in fictitious-time-step counter k [31], whereas the physical time step counter would still be n .

$$\begin{aligned}\mathbf{U}_i^{n+1,k+1} &= \mathbf{U}_i^{n+1,k} - \frac{\Delta\tau}{S_i} \sum_{T \in \cup\Delta_i} \left[B_i^T S_T \frac{d\mathbf{U}_i}{dt}(\mathbf{U}_i^{n+1,k}) + B_i^T \Phi^T(\mathbf{U}_i^{n+1,k}) \right] \\ &= \mathbf{U}_i^{n+1,k} - \frac{\Delta\tau}{S_i} \sum_{T \in \cup\Delta_i} [\alpha_i^T(\mathbf{U}_i^{n+1,k}) + B_i^T \Phi^T(\mathbf{U}_i^{n+1,k})].\end{aligned}\tag{5.17}$$

The alike alteration is made for the pseudo-time marching scheme in 3D by replacing S_i with V_i . The fictitious-time-step does not have any physical significance, but just play the role as iterative procedure, introduced by Jameson [30] firstly in the FV method called dual-time-stepping. In his original work, it was an implicit way of solving transient problem, with additional multistage Runge-Kutta pseudo-time iterations sandwiched between two consecutive time steps t^n and t^{n+1} . The advantage of pseudo-time marching scheme is that the order of accuracy in τ would not extirpate the accuracy of LDA scheme, even if it is just a first-order forward-Euler with central-lumping in pseudo-time iterations. The only disadvantage of this implicit solver is perforce more computational time is needed.

5.5. Time discretization

The last piece of information to consummate the full RD scheme is the time integration. Since the flux residual is of second-order-accurate, the time integration formula should be second-order-accurate in time to preserve the accuracy. There are three typical time discretization discussed here, namely the central-time (leapfrog) discretization, two-stage Runge-Kutta time-discretization and backward-time discretization. Referring to the analysis given in Section 5.1, if one chooses second-order time-integration formula, term-5 in Eq. (5.5a) would be eliminated.

1. Central-time discretization (Leap-Frog)

The time derivative is discretized as

$$\frac{d\mathbf{U}_i^n}{dt} = \frac{\mathbf{U}_i^{n+1} - \mathbf{U}_i^{n-1}}{2\Delta t} + O(\Delta t^2),$$

such that the Galerkin approach becomes explicit by the row-mass-lumping procedure

$$\mathbf{U}_i^{n+1} = \mathbf{U}_i^n - \frac{2\Delta t}{S_i} \sum_{T \in \cup\Delta_i} \Phi^T(\mathbf{U}^n).\tag{5.18}$$

The LW scheme appears ostensibly in forward-time integration, but is in fact having the flux and unsteady residuals evaluated as time-step $n + 1/2$

$$\frac{d\mathbf{U}_i^{n+\frac{1}{2}}}{dt} = \frac{\mathbf{U}_i^{n+1} - \mathbf{U}_i^n}{\Delta t} + O(\Delta t^2),\tag{5.19}$$

such that the LW-RD scheme after some manipulations gives

$$\mathbf{U}_i^{n+1} = \mathbf{U}_i^n - \frac{\Delta t}{S_i} \sum_{T \in \cup\Delta_i} B_i^T \Phi^T(\mathbf{U}^n),\tag{5.20}$$

with the fact that B_i^T has included the second-order time-correction based on data at \mathbf{U}^n .

The main drawback of this central-time discretization is the stability issue. The scheme is conditionally stable such that the physical time step Δt has to comply with the CFL condition, which is usually very small.

2. Two-stage Runge-Kutta time discretization

The leapfrog time-discretization is second-order-accurate, but might suffer some stability issues, especially for LDA scheme. There is another alternative for explicit time-discretization, known as the two-stage Runge-Kutta method. This numerical time integration is very familiar in the RD framework [44,63]. It is somehow like a predictor-corrector time-integration which requires the evaluation of intermediate time-step $\mathbf{U}_i^{n+1/2}$ to calculate the flux residual. After that, the nodal update from \mathbf{U}_i^n to \mathbf{U}_i^{n+1} is carried out explicitly. This time-discretization formula is second-order-accurate locally.

In RD-LDA scheme, the lumping should take effects on the two-stage Runge-Kutta method

$$\mathbf{U}_i^{n+\frac{1}{2}} = \frac{\Delta t}{2} \left(\sum_{T \in \cup\Delta_i} S_T B_i^T \right)^{-1} \sum_{T \in \cup\Delta_i} \left[\frac{S_T}{\Delta t/2} B_i^T \mathbf{U}_i^n - \sum_{T \in \cup\Delta_i} B_i^T \Phi^T(\mathbf{U}^n) \right],\tag{5.21a}$$

$$\mathbf{U}_i^{n+1} = \Delta t \left(\sum_{T \in \cup\Delta_i} S_T B_i^T \right)^{-1} \sum_{T \in \cup\Delta_i} \left[\frac{S_T}{\Delta t} B_i^T \mathbf{U}_i^n - \sum_{T \in \cup\Delta_i} B_i^T \Phi^T(\mathbf{U}^{n+\frac{1}{2}}) \right].\tag{5.21b}$$

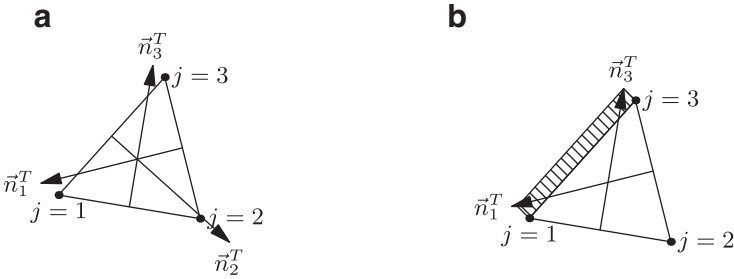


Fig. 13. (a) The flux residual for all elements in interior domain. (b) The elements abutted with PEC boundary. No electric curl is allowed to penetrate the PEC boundary, as described by Eq. (5.26b).

There are several remarks regarding the inversion of the row-mass-lumped component in equation (5.21). Firstly, since Maxwell's equations are linear hyperbolic system, unlike the Euler equation, $\sum_{T \in \Delta_i} S_T B_i^T$ will always be the same for every time step t^n , as long as μ and ε do not change with time. Secondly, $\sum_{T \in \Delta_i} S_T B_i^T$ cannot be the same for all triangular elements, unless the mesh is generated in some very structured orientation, such as the right-running grid or equilateral grid. Lastly, $\sum_{T \in \Delta_i} S_T B_i^T$ is not the same for all triangles in general, therefore it is evaluated numerically for all the computations in this work.

3. Backward-time discretization The time derivative is discretized as

$$\frac{d\mathbf{U}_i^n}{dt} = \frac{3\mathbf{U}_i^{n+1} - 4\mathbf{U}_i^n + \mathbf{U}_i^{n-1}}{2\Delta t} + O(\Delta t^2), \quad (5.22)$$

and all the RD schemes employing such a time integration formula are implicit. The Galerkin-RD scheme is to be solved iteratively as

$$\mathbf{U}_i^{n+1,k+1} = \mathbf{U}_i^{n+1,k} - \frac{\Delta\tau}{S_i} \left[S_i \frac{3\mathbf{U}_i^{n+1,k} - 4\mathbf{U}_i^n + \mathbf{U}_i^{n-1}}{2\Delta t} + \sum_{T \in \Delta_i} \frac{I}{3} \Phi^T(\mathbf{U}^{n+1,k}) \right], \quad (5.23)$$

while the LDA scheme reads

$$\mathbf{U}_i^{n+1,k+1} = \mathbf{U}_i^{n+1,k} - \frac{\Delta\tau}{S_i} \sum_{T \in \Delta_i} \left[B_i^T S_T \frac{3\mathbf{U}_i^{n+1,k} - 4\mathbf{U}_i^n + \mathbf{U}_i^{n-1}}{2\Delta t} + B_i^T \Phi^T(\mathbf{U}^{n+1,k}) \right]. \quad (5.24)$$

Both of the schemes are implicit, but they are unconditionally stable, such that they do not necessary need to fulfill the CFL condition. In other words, the step Δt could be made larger.

The generalization to three-dimensional is rather straightforward to apply.

5.6. Boundary condition

The perfect electric conductor (PEC) boundary condition is a media interface where all tangential electric field should go to zero. Metallic objects are electric conductors. Similar as to the Meissner effect in superconductor, the magnetic field should be zero inside the PEC. The tangential electric field is zero along the boundary, but the tangential magnetic field is not. Hence, there is no variation in tangential electric field across the boundary, but the tangential magnetic field is discontinuous across PEC boundary. The PEC boundary is described by

$$-\mathbf{n} \times \mathbf{E} = 0, \quad (5.25)$$

the negative sign is because of the scaled normal in RD framework which points inwardly. The flux residual for elements in interior domain and for boundary elements (say if $j = 1$ and $j = 3$ fall on the boundary as shown in Fig. 13b) are given as

$$\frac{1}{\mu} \Phi^{T(\Omega)}(\mathbf{E}) = \frac{1}{2}(-\mathbf{n}_1) \times (\mathbf{E}_3 + \mathbf{E}_2) + \frac{1}{2}(-\mathbf{n}_2) \times (\mathbf{E}_3 + \mathbf{E}_1) + \frac{1}{2}(-\mathbf{n}_3) \times (\mathbf{E}_1 + \mathbf{E}_2) \quad (5.26a)$$

and

$$\frac{1}{\mu} \Phi^{T(\Omega)}(\mathbf{E}) = \frac{1}{2}(-\mathbf{n}_1) \times (\mathbf{E}_3 + \mathbf{E}_2) + \frac{1}{2}(-\mathbf{n}_3) \times (\mathbf{E}_1 + \mathbf{E}_2) \quad (5.26b)$$

respectively. The negative sign is to accompany the inward scaled normal \mathbf{n}_j^T . The extension to three-dimension is rather straightforward.

In order to achieve explicit time-marching scheme, the weak imposition of boundary condition is adapted. Only three test cases in this work involve the PEC boundary condition, and their details of implementation are given as following.

3D Rectangular waveguide (TM mode)

- i. The three-dimensional version of flux residual $\Phi^{T(\partial\Omega)}(\mathbf{E})$ has to be used for edges along $x = 0$, $x = 1$, $y = 0$ and $y = 1$.
- ii. Besides that, this test case is a TM mode propagation, and $H_z = 0$ for all domain Ω .
- iii. Additional weak imposition of tangential electric field components at the surface is also needed so that the sharp corners of rectangular waveguide can still capture the flux properly.

$$\begin{aligned} E_z &= 0 \quad \text{at } \{x = 0, x = 1, y = 0, y = 1\} \\ E_x &= 0 \quad \text{at } \{y = 0, y = 1\} \\ E_y &= 0 \quad \text{at } \{x = 0, x = 1\} \end{aligned} \tag{5.27}$$

2D Scattering (TM mode)

- i. The boundary flux residual of Eq. (5.26b) is used for elements located at the interior radius that bounds the hollow cavity (perfect conductor) $\rho = a$.
- ii. $E_z = 0$ at $\rho = a$.

6. Results and discussions

The profundity of knowledge in electrodynamics has left the readers with substantial number of test cases, some of which are very sophisticated. In this work, only a few very simple examples are tested, four for the two-dimensional cases and one three-dimensional test case. All of the test cases are provided with analytical solution, so that one could ascertain with the numerical results, and thus the second-order-accuracy of linear-preserving RD scheme could be verified from the L_2 -errors.

6.1. Mesh-dependency study (2D Parallel-plate waveguide in TM mode)

One of the advantage of RD scheme is that the scheme is less affected by the irregularity of the mesh. Recalling from the fundamental construction of RD scheme, the compactness of the scheme is asserted by the nodal update of node i involving only flux residual Φ^T from adjoining cells, unlike certain FV schemes which require gradient reconstruction or interpolation that entails information from second layer of neighboring cells. This footing of compact stencil is deemed to be the main cause that compact scheme, such as the RD scheme is less influenced by the arrangement of the grids.

Hence, a parallel-plate waveguide in 2D is adduced to observe the mesh-dependency of RD scheme. This test case has its wave profiles (electric field components) propagating in x -direction, but oscillating as standing waves in y -direction. The H_x , H_y and E_z components of this 2D waveguide are given as

$$H_x = j \frac{E_0 \kappa_n}{\omega \mu} \cos(\kappa_n y) \exp(j(\omega t - \beta_m x)), \tag{6.1a}$$

$$H_y = -j \frac{E_0 \beta_m}{\omega \mu} \sin(\kappa_n y) \exp(j(\omega t - \beta_m x)), \tag{6.1b}$$

$$E_z = E_0 \sin(\kappa_n y) \cos(\omega t - \beta_m x). \tag{6.1c}$$

The computational domain of $\Omega \in \{x : -1 \leq x \leq 1, y : -1 \leq y \leq 1\}$ gives $b = 1 - (-1) = 2$, which is the distance between $y = -1$ and $y = 1$. The other parameters are given as

$$\beta_m = \text{propagation coefficient in } x\text{-direction} = 2\pi, \tag{6.2a}$$

$$\kappa_n = \text{number of standing waves bounded between } -1 \leq y \leq 1 = \frac{n\pi}{b}, \quad n = 0, 1, 2, \dots, \tag{6.2b}$$

$$k^2 - \beta_m^2 = \kappa_n^2 \implies k^2 = \sqrt{\beta_m^2 + \kappa_n^2}. \tag{6.2c}$$

The angular frequency ω could be determined from relation of

$$k^2 = \omega^2 \mu \epsilon. \tag{6.2d}$$

The test begins with anisotropic mesh, which is a square structured grid, each halved by an alternating diagonal, giving the mesh the semblance to diamond-shaped. The order-of-accuracy should be close to 2 for this structured grid. The positions of nodes are then shifted randomly within the range of $0.4\Delta x$ from their original locations, and the randomized grid is then procured. The final time is set to be t_{100} . The values for $m = 2$ and $n = 2$ are chosen such as the wave profiles are symmetrical across the boundaries, and therefore the periodic boundary condition which is usually be seen in CFD community can be utilized.

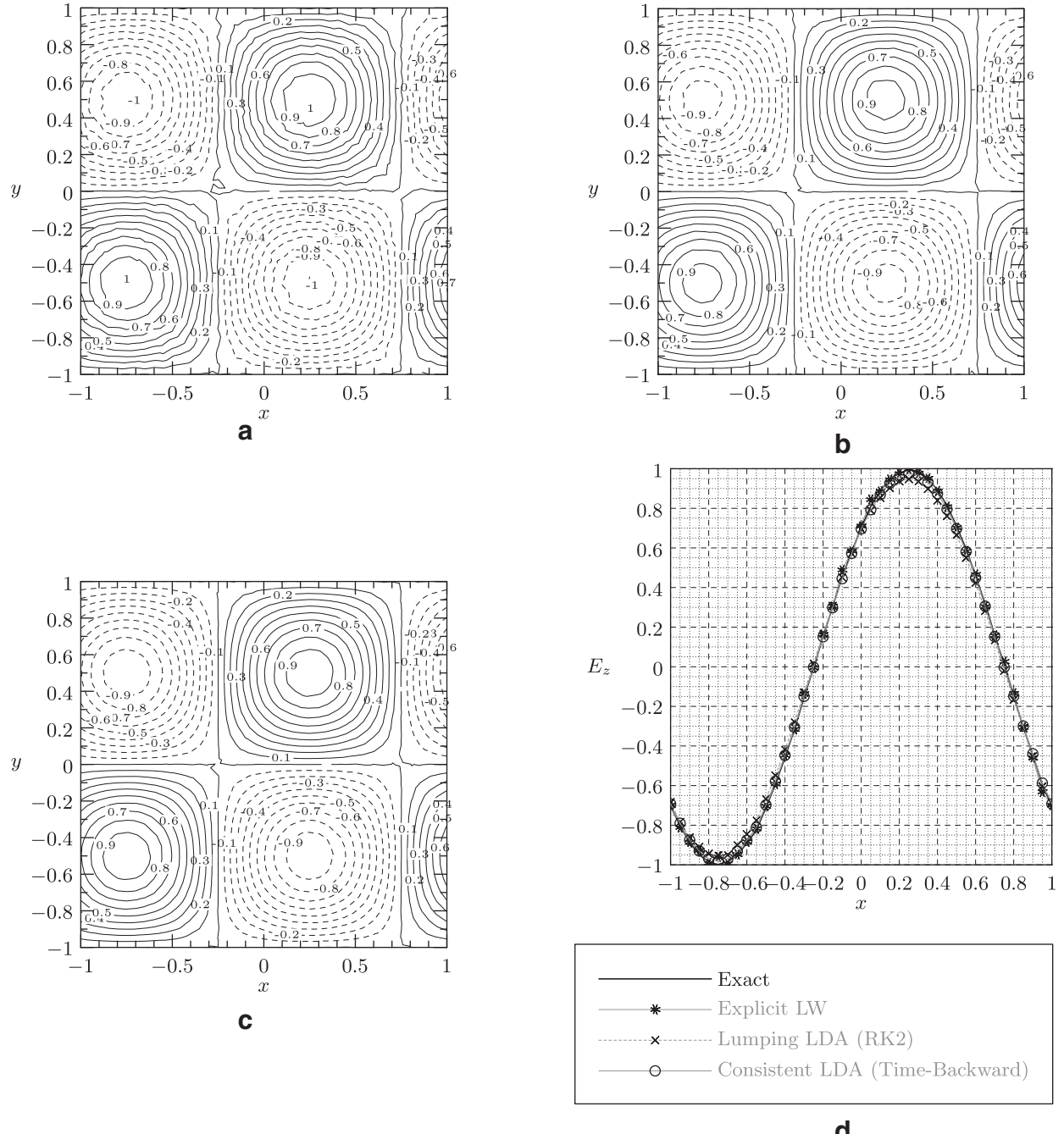


Fig. 14. The mesh-dependency study in 2D, with density plots for the coarsest randomized grid 40×40 . The density plot of E_z after 100 time steps for (a) Lax-Wendroff scheme, (b) RK2 mass-lumping LDA scheme and (c) consistent time-backward LDA scheme. The slice across $y = 0.75$ is given in (d).

The contour plot of E_z for the study of mesh-irregularity in randomized grid are given in Fig. 14. A portion of anisotropic grid and its corresponding randomized grid are given in Fig. 15. The order-of-accuracy is expected to detract from the second-order upon the distortion of the anisotropic mesh, but still maintaining at about 2 for LW scheme and Galerkin approach. However, the LDA scheme does not suffer much drop than the former two, may be due to its upwinding distribution. The L_2 -errors for this study of mesh-dependency are compared in Fig. 16, and the gross computational time for this mesh-dependency study is given in Fig. 17. The magnitudes for each L_2 -error are tabulated in Table 2. It is from the density plots in Fig. 14 which show that upwind-LDA scheme has smoother wave profile than the explicit LW scheme. The L_2 -error slope in Fig. 16b slightly tapers off when the randomized grid is refined, mainly due to some of the triangles are highly skewed as the distance between vertices are getting extremely close.

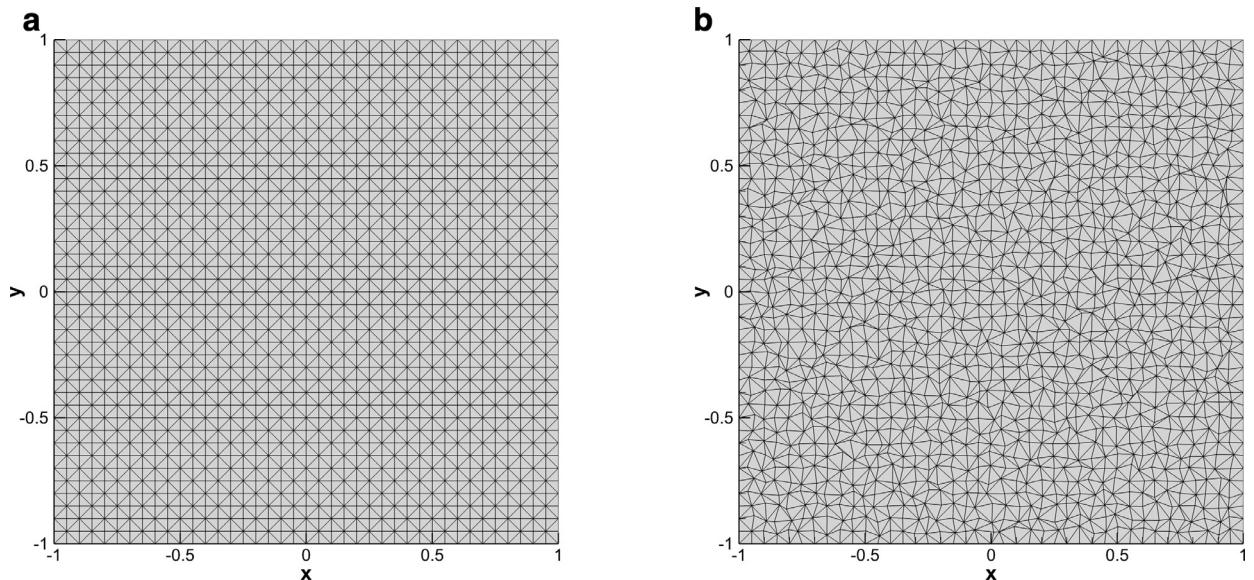


Fig. 15. (a) An anisotropic mesh in 2D. (b) The corresponding mesh randomized from the structured anisotropic grid.

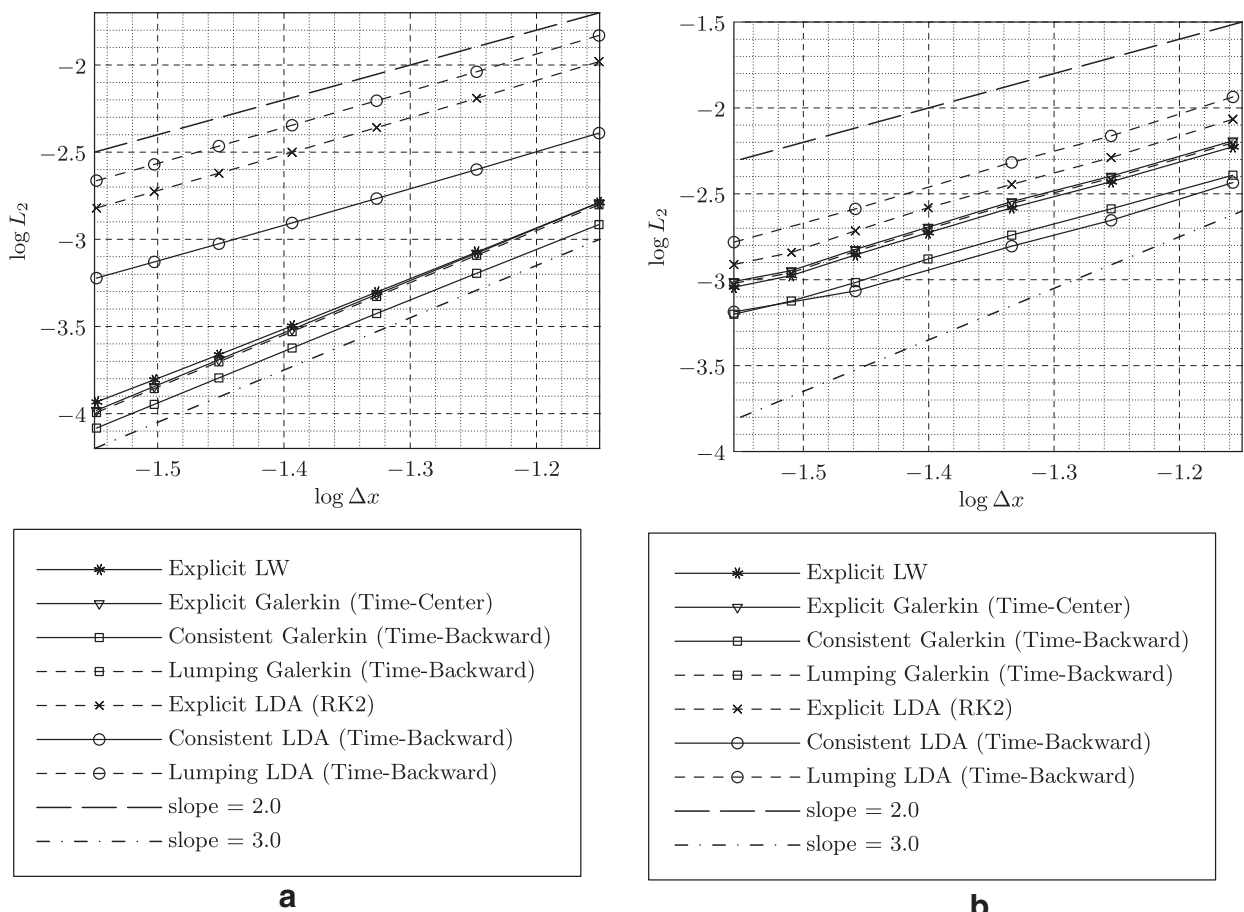


Fig. 16. The L_2 -errors for (a) the anisotropic grid in 2D, (b) the randomized grid in 2D. The gradient of the slopes are tabulated in Table 2.

Table 2

The gradient of the $\log L_2$ -errors against the $\log \Delta x$ for structured grid and randomized grid after 40 time steps.

RD schemes	Anisotropic grid	Randomized grid
LW scheme	2.87568	2.08701
Galerkin (Explicit Leapfrog)	3.03449	2.09575
Galerkin (Lumping Backward-Time)	2.9957	2.09441
Galerkin (Consistent Backward-Time)	2.93681	2.0626
LDA (Explicit RK2)	2.10785	2.14026
LDA (Lumping Backward-Time)	2.09149	2.11523
LDA (Consistent Backward-Time)	2.08829	1.91414

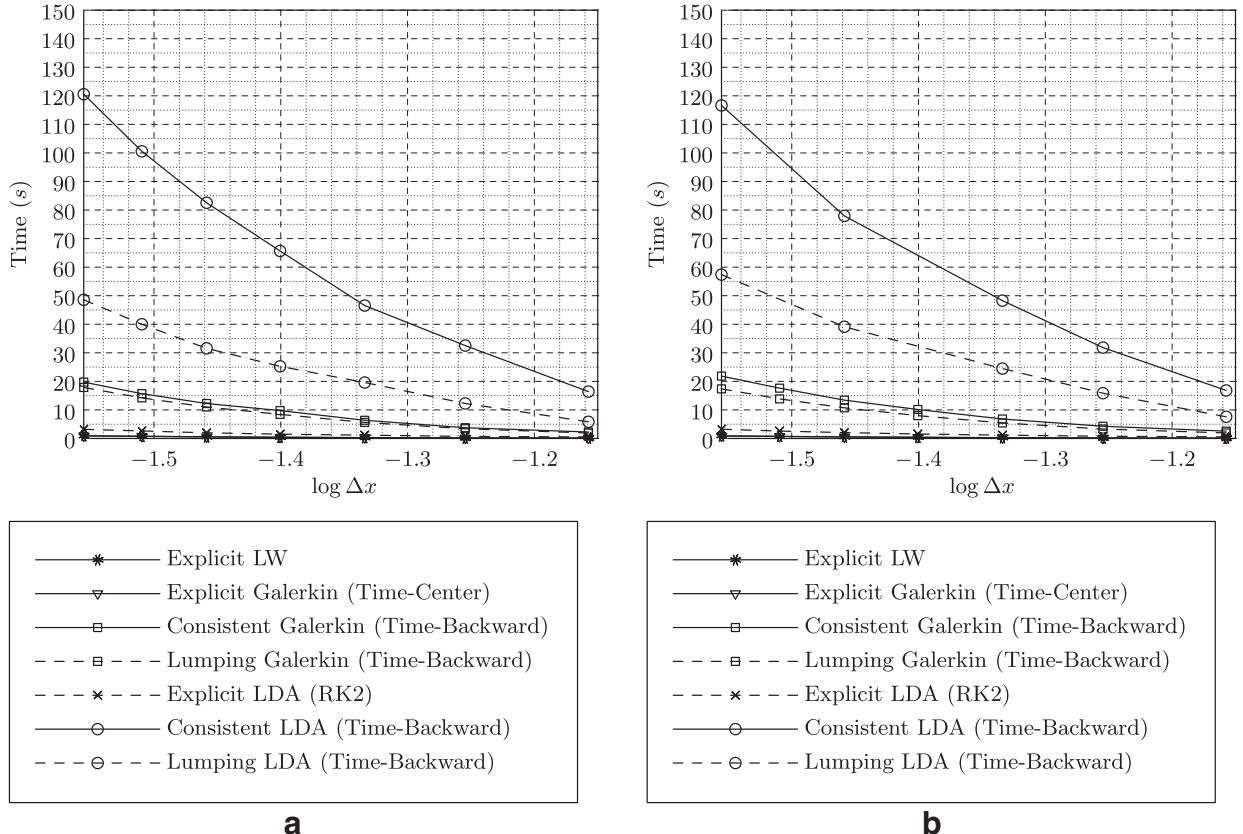


Fig. 17. The computational execution time of different RD schemes on (a) anisotropic mesh, and (b) randomized grid. This is for the study of mesh-dependency using parallel-plate waveguide test case.

6.2. 2D radiation (TM mode)

The simplest radiation problem comes from a long wire with current I_e running in $+z$ -direction. This is not even a dipole radiation, so that procuring the exact solution is easy without the need of long-range or short-range approximation. The wire is assumed to occupy the space of a single point and is infinitely long. The solution for outward-traveling radiation problem comprises of Hankel function of second kind $H_v^{(2)}(\beta\rho) = J_v(\beta\rho) - jY_v(\beta\rho)$. Both the electric and magnetic fields at the source point is infinite, mathematically due to the Bessel function of second kind $Y_v(\rho = 0) \rightarrow \infty$. This will engender the failure of the numerical scheme to converge. Therefore during the simulation, the values of the fields at each time step was replaced with their analytical solutions in the vicinity of the point $\rho \rightarrow 0$. One would find in this setting a radiation emanates from the center of the domain, and the boundaries are left without any further treatment as the perpetual radiation from the center will always replenish the boundaries with new wavefronts. This example is given in [6] as

$$E_z = -I_e \frac{\omega\mu}{4} H_0^{(2)}(\beta\rho) \exp(j\omega t), \quad (6.3a)$$

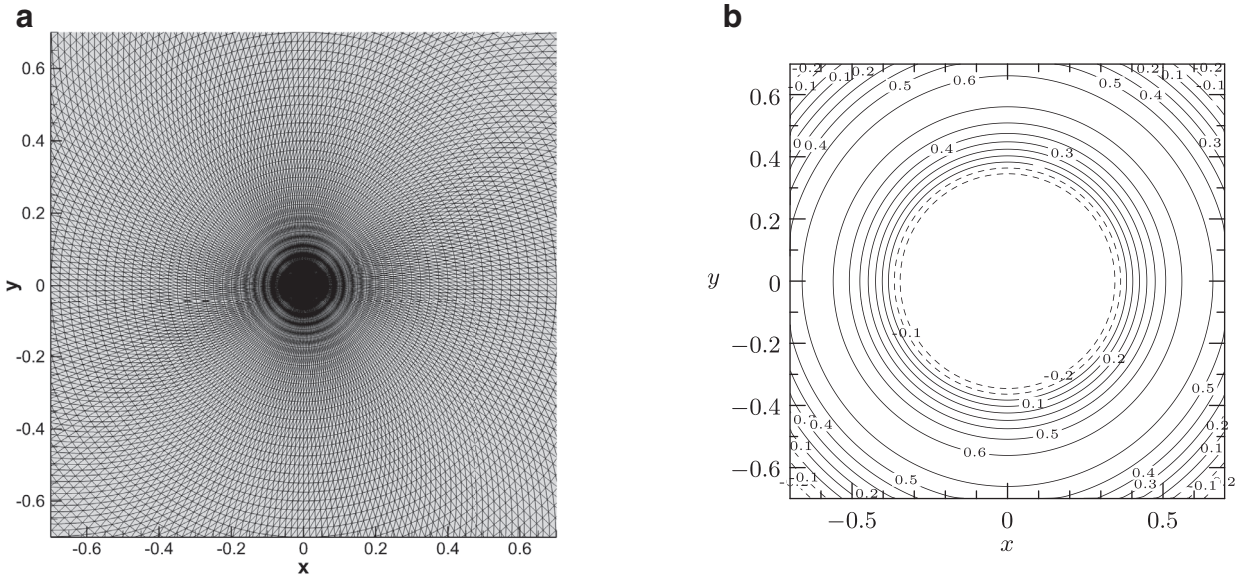


Fig. 18. (a) The mesh for 2D radiation problem. (b) The exact initial E_z at $t = 0$ contour plot for 2D radiation problem.

$$H_\phi = jI_e \frac{\beta}{4} H_0^{(2)\prime}(\beta\rho) \exp(j\omega t). \quad (6.3b)$$

where

$$I_e = \text{electric current of the wire} = 1, \quad (6.4a)$$

$$\beta = \text{propagation coefficient in radial direction} = 2\pi, \quad (6.4b)$$

$$\omega = \text{angular frequency}; \quad \beta^2 = \omega^2 \mu \epsilon \implies \omega = \frac{\beta}{\sqrt{\mu \epsilon}}, \quad (6.4c)$$

$$\mu = \text{permeability} = 1, \quad (6.4d)$$

$$\epsilon = \text{permittivity} = 1. \quad (6.4e)$$

$H_0^{(2)\prime}(\beta\rho) = J'_0(\beta\rho) - jY'_0(\beta\rho)$ being the radial derivative of the Hankel function, which follows closely the properties of Bessel function. The following definitions for derivative and recursive of Hankel function has to be used

$$H_v^{(2)\prime}(\beta\rho) = \frac{1}{2} [H_{v-1}^{(2)}(\beta\rho) - H_{v+1}^{(2)}(\beta\rho)], \quad (6.5a)$$

$$\frac{v}{\rho} H_v^{(2)}(\beta\rho) = \frac{1}{2} [H_{v-1}^{(2)}(\beta\rho) + H_{v+1}^{(2)}(\beta\rho)]. \quad (6.5b)$$

The x - and y -components of \mathbf{H} can be obtained from $H_\phi \hat{\phi}$ as

$$H_x = -H_\phi \sin(\phi), \quad (6.6a)$$

$$H_y = H_\phi \cos(\phi). \quad (6.6b)$$

The mesh generated by the authors for this two dimension radiation problem is shown in Fig. 18a and the initial wave profile for E_z in Fig. 18b. Fig. 19 shows the numerical results for two-dimensional radiation problem by lumping LDA scheme with RK2 time-marching scheme. The cross-sectional plots at $t = 0.25$ and $t = 0.5$ are given in Fig. 20. The explicit Lax-Wendroff scheme has some very accurate results, compared with the upwind LDA schemes. It seems to outperform the upwind RD-LDA scheme, especially in the vicinity of extrema (or turning points). The Galerkin schemes also work for this test case, both in backward-time discretization or leapfrog time-discretization. However, the numerical results from Galerkin schemes are not shown here, because their outcomes are very close to those of the Lax-Wendroff scheme.

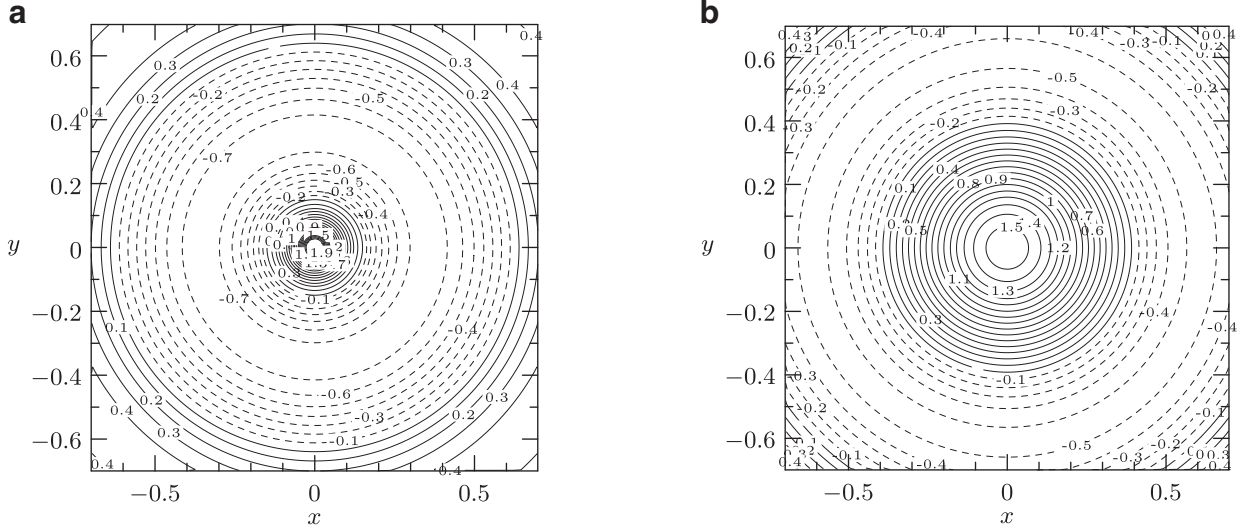


Fig. 19. The density plot of E_z in radiation problem using RK2 mass-lumping LDA scheme at (a) $t = 0.25$, (b) $t = 0.5$.

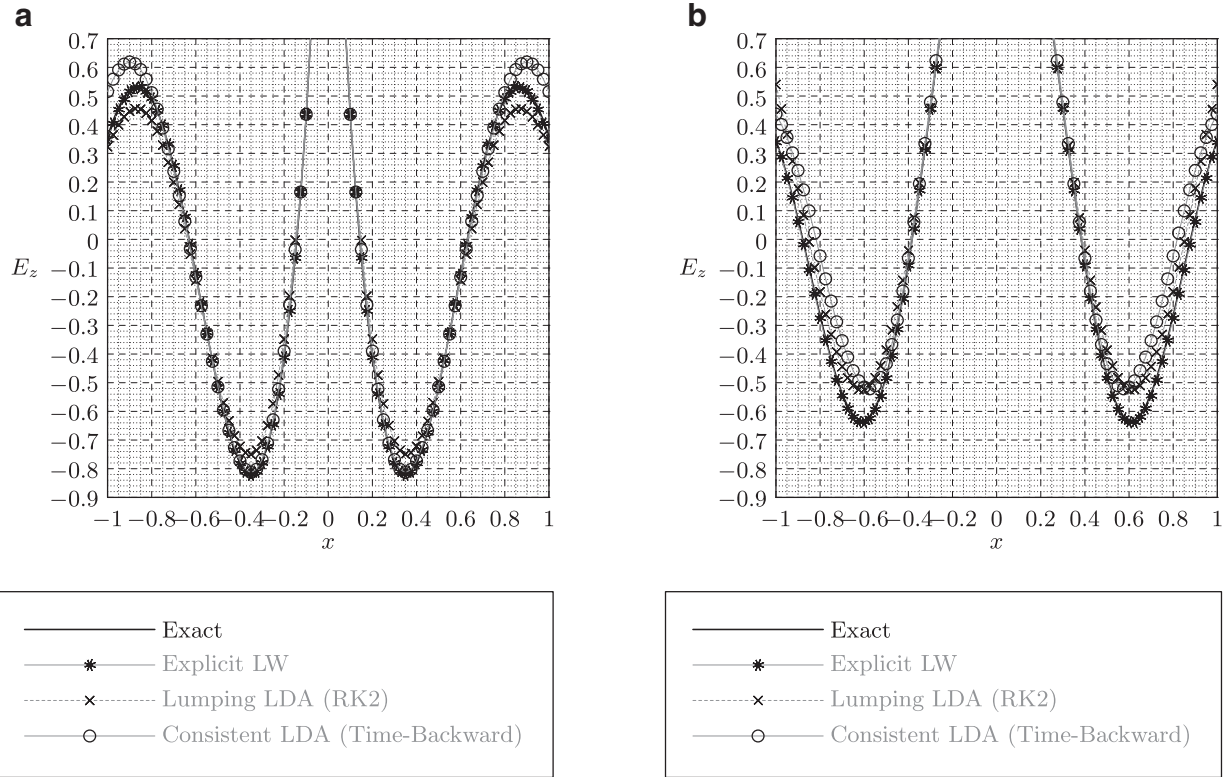


Fig. 20. The cross-sectional plot ($y = 0$) of E_z in radiation problem at (a) $t = 0.25$, (b) $t = 0.5$. The region close to $x = 0$ is not shown as the wave signal blows up to infinity, due to the $Y_v(\beta\rho)$ -term of Bessel function second kind. Moreover, this domain is considered as the source region.

6.3. 2D Hertzian-dipole (TE mode)

Another 2D example of radiation is the Hertzian dipole problem [6,62]. The electrical dipole is more physical than the existence of magnetic dipole in real-time application, and therefore is presented here as Hertzian dipole of TE mode. There are two electrical charges pinned on $(+0.5, 0)$ and $(-0.5, 0)$, each having an opposite charge but equal in magnitude. Imagining that these two opposite charges are bridged together via a negligible thin wire, and the relentless swapping of these positive and negative terminals give rise to electromagnetic waves rippling away from the sources. The interference of wavefronts

from these two electrical sources from a pattern, which can be represented by Eq. (6.7)

$$E_r = \Re \left\{ \frac{I_0 d}{2\pi} \sqrt{\frac{\mu}{\varepsilon}} \cos \theta \left(\frac{1}{r^2} - j \frac{1}{kr^3} \right) \exp j(\omega t - kr) \right\} \quad (6.7a)$$

$$= \frac{I_0 d}{2\pi} \sqrt{\frac{\mu}{\varepsilon}} \cos \theta \left[\frac{\cos(\omega t - kr)}{r^2} + \frac{\sin(\omega t - kr)}{kr^3} \right],$$

$$E_\theta = \Re \left\{ \frac{I_0 d}{4\pi} \sqrt{\frac{\mu}{\varepsilon}} \sin \theta \left(\frac{1}{r^2} + j \frac{k}{r} - j \frac{1}{kr^3} \right) \exp j(\omega t - kr) \right\} \quad (6.7b)$$

$$= \frac{I_0 d}{4\pi} \sqrt{\frac{\mu}{\varepsilon}} \sin \theta \left[\frac{\cos(\omega t - kr)}{r^2} + \frac{\sin(\omega t - kr)}{kr^3} - \frac{k \sin(\omega t - kr)}{r} \right],$$

$$H_\phi = \Re \left\{ \frac{I_0 d}{4\pi} \sin \theta \left(\frac{1}{r^2} + j \frac{k}{r} \right) \exp j(\omega t - kr) \right\} \quad (6.7c)$$

$$= \frac{I_0 d}{4\pi} \sin \theta \left[\frac{\cos(\omega t - kr)}{r^2} - \frac{k \sin(\omega t - kr)}{r} \right],$$

where

$$\lambda = \text{wavelength} = 1, \quad (6.8a)$$

$$k = \text{wavenumber} = \frac{2\pi}{\lambda}, \quad (6.8b)$$

$$\omega = \text{angular frequency} \iff k^2 = \omega^2 \mu \varepsilon, \quad (6.8c)$$

$$I_0 = \text{electric current of the thin wire} = 1, \quad (6.8d)$$

$$d = \text{separation distance between the dipoles} = 1.0, \quad (6.8e)$$

$$\mu = \text{permeability} = 1, \quad (6.8f)$$

$$\varepsilon = \text{permittivity} = 1. \quad (6.8g)$$

(6.7) are given in spherical coordinates, and could be transformed into Cartesian coordinates via

$$E_x = \begin{cases} E_\theta \cos \theta + E_r \sin \theta, & x \geq 0 \\ -E_\theta \cos \theta - E_r \sin \theta, & x < 0 \end{cases} \quad (6.9a)$$

$$E_y = E_\theta \cos \theta - E_r \sin \theta, \quad (6.9b)$$

$$H_z = \begin{cases} -H_\phi, & x \geq 0 \\ H_\phi, & x < 0 \end{cases} \quad (6.9c)$$

Likewise to the previous example, the contour line plot of H_z after $t = 0.5$ and $t = 1.0$ for Hertzian dipole problem are shown in Fig. 22 for lumped upwind LDA scheme. On the other hand, a couple of cross-sectional plots for all the three RD techniques being tested here are given in Fig. 23. The mesh in use for this test case is very dense at $x = -0.5$ and $x = +0.5$ as shown in Fig. 21a as they have to capture the point source effectively. The initial wave profile for H_z is also given in Fig. 21b. In this test case, the implicit consistent-LDA scheme outshines the explicit lumped-LDA scheme. This happens because the peaks of the wave profile are sharper than in the 2D radiation problem presented in previous section. Some numerical treatments are imposed at radius $r < 1.0$, to make sure that all the nodes within this domain are provided with their analytical solutions for every time step. This is because at radius $r \rightarrow 0$, the fields will blow up to infinity due to the $1/r$, $1/r^2$ or $1/r^3$ -terms, which comply with the mathematical theory of radiation.

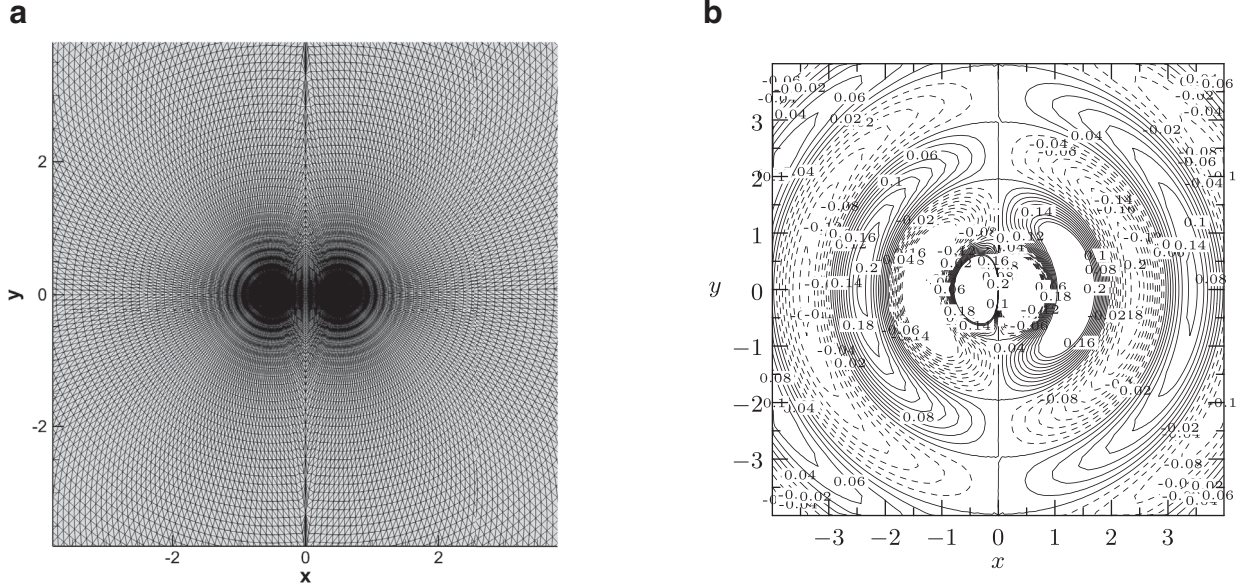


Fig. 21. (a) The mesh for 2D Hertzian dipole problem. (b) The exact initial H_z at $t = 0$ contour plot for 2D Hertzian dipole problem.

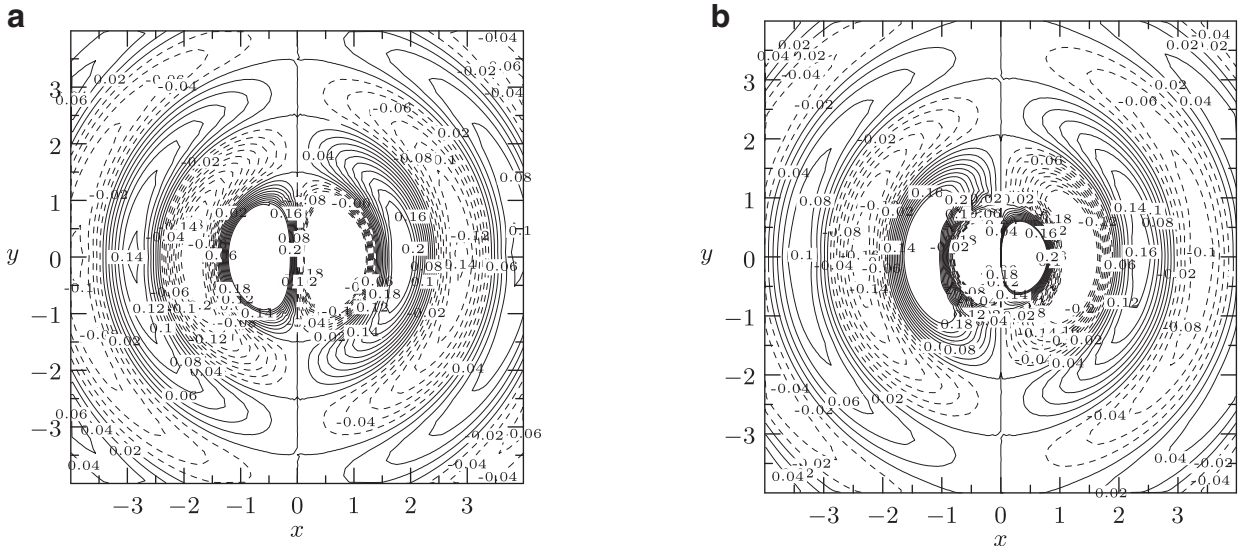


Fig. 22. The density plot of H_z in Hertzian dipole problem using RK2 mass-lumping LDA scheme at (a) $t = 0.5$, (b) $t = 1.0$.

6.4. 2D scattering by circular cylinder (TM Mode)

The TM mode in two-dimensional constitutes of three conserved variables: H_x , H_y , E_z (or rather H_ρ , H_ϕ , E_z in cylindrical coordinates). To be general, the RD scheme discretizes the problem in Cartesian coordinates, whereas the analytical solutions to this scattering problem comprise of Bessel function in cylindrical coordinates. Anyhow, this is not a big trouble as the cylindrical and Cartesian coordinates could be resolved into one another using trigonometric relations. Essentially, E_z component is traversing in the positive x -direction, when it reaches a cylindrical obstacle that interposed in its propagating path, all the H_x , H_y and E_z components will yaw in all directions. Hence, the analytical solutions are the amalgamation of the incident waves H_ρ^i , H_ϕ^i , E_z^i and the scattered waves H_ρ^s , H_ϕ^s , E_z^s [6]. The cylinder would not allow the electromagnetic waves to penetrate it, and its surface is coated with a perfect conducting material such that the PEC boundary condition as give in Section 5.6 is applicable

$$H_\rho = -\frac{E_0}{\omega\mu} \sum_{\nu=-\infty}^{+\infty} \frac{\nu}{\rho} j^{-\nu} \left[J_\nu(\beta\rho) - \frac{J_\nu(\beta a)}{H_\nu^{(2)}(\beta a)} H_\nu^{(2)}(\beta\rho) \right] \exp j(\nu\phi + \omega t), \quad (6.10a)$$

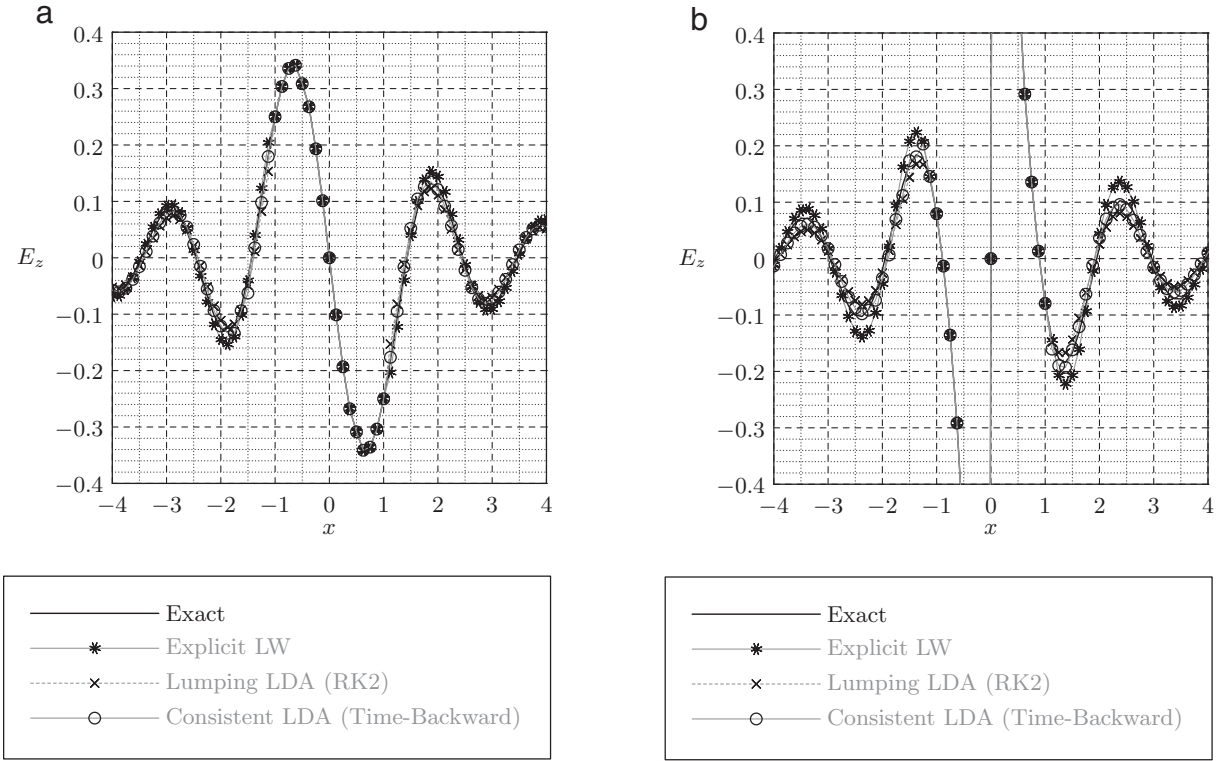


Fig. 23. The cross-sectional plot ($y = 0$) of H_z in Hertzian dipole at (a) $t = 0.5$, (b) $t = 1.0$. Peaks close to the origin are trimmed off as they tend to be infinite. Thus, values within $r \leq 1.0$ are always set to their analytical solutions, like a wavefront that keeps emanating from the source.

$$H_\phi = -\frac{\beta E_0}{\omega \mu} \sum_{v=-\infty}^{+\infty} j^{1-v} \left[J'_v(\beta \rho) - \frac{J_v(\beta a)}{H_v^{(2)}(\beta a)} H_v^{(2)\prime}(\beta \rho) \right] \exp j(v\phi + \omega t), \quad (6.10b)$$

$$E_z = E_0 \sum_{v=-\infty}^{+\infty} j^{-v} \left[J_v(\beta \rho) - \frac{J_v(\beta a)}{H_v^{(2)}(\beta a)} H_v^{(2)}(\beta \rho) \right] \exp j(v\phi + \omega t). \quad (6.10c)$$

Pay heed to the terms of $(v/\rho)H_v^{(2)}$ are to be evaluated using the recurrence relation similar to that of Eq. (6.5b). The transformation from cylindrical to Cartesian coordinates takes the form of

$$H_x = H_\rho \cos \phi - H_\phi \sin \phi, \quad (6.11a)$$

$$H_y = H_\rho \sin \phi + H_\phi \cos \phi. \quad (6.11b)$$

As for this test case, the contour plot of E_z would already do a good comparison between different RD schemes. The initial E_z of Eq. (6.10) and the meshing for this problem are given in Fig. 24. For the sake of comparison, the analytical solution and numerical solutions from few selected RD schemes are presented side-by-side for time $t = 0.4$ in Fig. 25. Similar layout for analytical solution and numerical RD solutions at time $t = 0.8$ is given in Fig. 26. Since the mass-lumping effect is one of the investigation aspect in this work, therefore the E_z wave profiles with and without mass-lumping are given in (c) and (d), respectively, in Figs. 25 and 26. Having seen the benchmark analytical solutions and also their numerical results, the space-centered RD-LW produces wave profile which lagged a bit, especially right behind the circular cylinder. The salient implication from the numerical results in Figs. 25c-d and Figs. 26c-d is that explicitly lumped LDA scheme is capable of giving wave pattern as nice as the implicit consistent LDA scheme to the exact results, although the accuracy is expected to drop quicker as time goes along due to the row-mass-lumping procedure. The last words for the performance of RD scheme in this 2D scattering problem is that even though RD-LDA scheme has successfully produced less-diffusive numerical results for E_z , the approximate solutions for H_x and H_y components are not as accurate as its E_z counterpart.

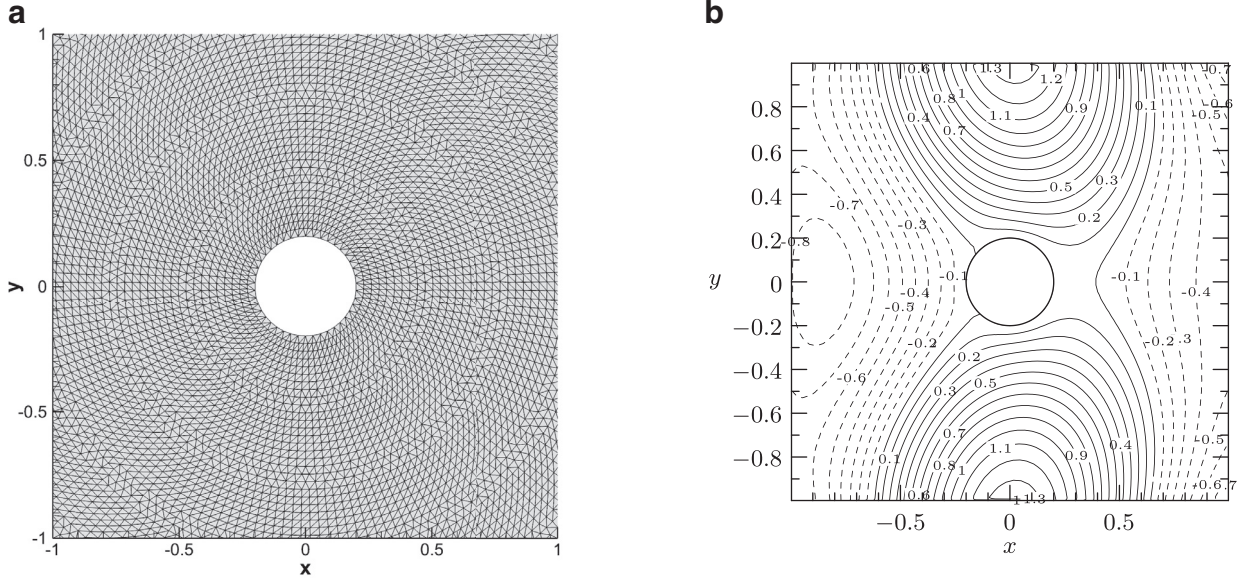


Fig. 24. (a) The mesh for 2D scattering problem. The (b) initial density plot of E_z .

6.5. 3D rectangular waveguide (TM Mode)

Examples of RD scheme in 3D are rather limited in the literature. It is understood that the 3D examples are more tangible in real-time application, and hence the 3D waveguide problem is studied here. The domain is taken to be $[0, 1] \times [0, 1] \times [0, 0.5]$ where the x and y -limits spanned from 0 to +1, while the propagating z -axis starts from 0 to 0.5.

Three variations on the size of structured tetrahedral mesh are tested, starting from $40 \times 40 \times 20$, $52 \times 52 \times 26$ and $64 \times 64 \times 32$, to justify the order-of-accuracy of linear-preserving RD scheme. The coarsest mesh of the rectangular waveguide comprises of 192000 tetrahedral elements whereas the finest mesh of the rectangular waveguide constituted by 786432 tetrahedral elements. The side boundaries along $x = 0, x = 1, y = 0, y = 1$ are incorporated with PEC boundary condition as has been described in Section 5.6. Similarly, the cross-sectional plane at $z = 0$ is always provided with incoming electromagnetic waves since it is an inflow boundary. The outflow boundary at $z = 0.5$ does not require any extra feeding of data in hyperbolic system. The derivation of the analytical solutions could be found in [23,40,41], and is just listed hereby as

$$E_{zmn}(x, y, z, t) = E_0 \sin(\kappa_m x) \sin(\kappa_n y) \cos(\omega t - \beta z), \quad (6.12a)$$

$$H_{zmn}(x, y, z, t) = 0, \quad (6.12b)$$

$$H_{xmn}(x, y, z, t) = -\frac{\omega \epsilon \kappa_n}{\kappa_{mn}^2} E_0 \sin(\kappa_m x) \cos(\kappa_n y) \sin(\omega t - \beta z), \quad (6.12c)$$

$$H_{ymn}(x, y, z, t) = \frac{\omega \epsilon \kappa_m}{\kappa_{mn}^2} E_0 \cos(\kappa_m x) \sin(\kappa_n y) \sin(\omega t - \beta z), \quad (6.12d)$$

$$E_{xmn}(x, y, z, t) = \frac{\beta \kappa_m}{\kappa_{mn}^2} E_0 \cos(\kappa_m x) \sin(\kappa_n y) \sin(\omega t - \beta z), \quad (6.12e)$$

$$E_{ymn}(x, y, z, t) = \frac{\beta \kappa_n}{\kappa_{mn}^2} E_0 \sin(\kappa_m x) \cos(\kappa_n y) \sin(\omega t - \beta z). \quad (6.12f)$$

and each of the symbols represent physical quantity such as following:

$$\omega = \text{angular frequency}, \quad (6.13a)$$

$$\kappa_m = \frac{m\pi}{a}, m = 1, 2, 3, \dots; \quad \kappa_n = \frac{n\pi}{b}, n = 1, 2, 3, \dots, \quad (6.13b)$$

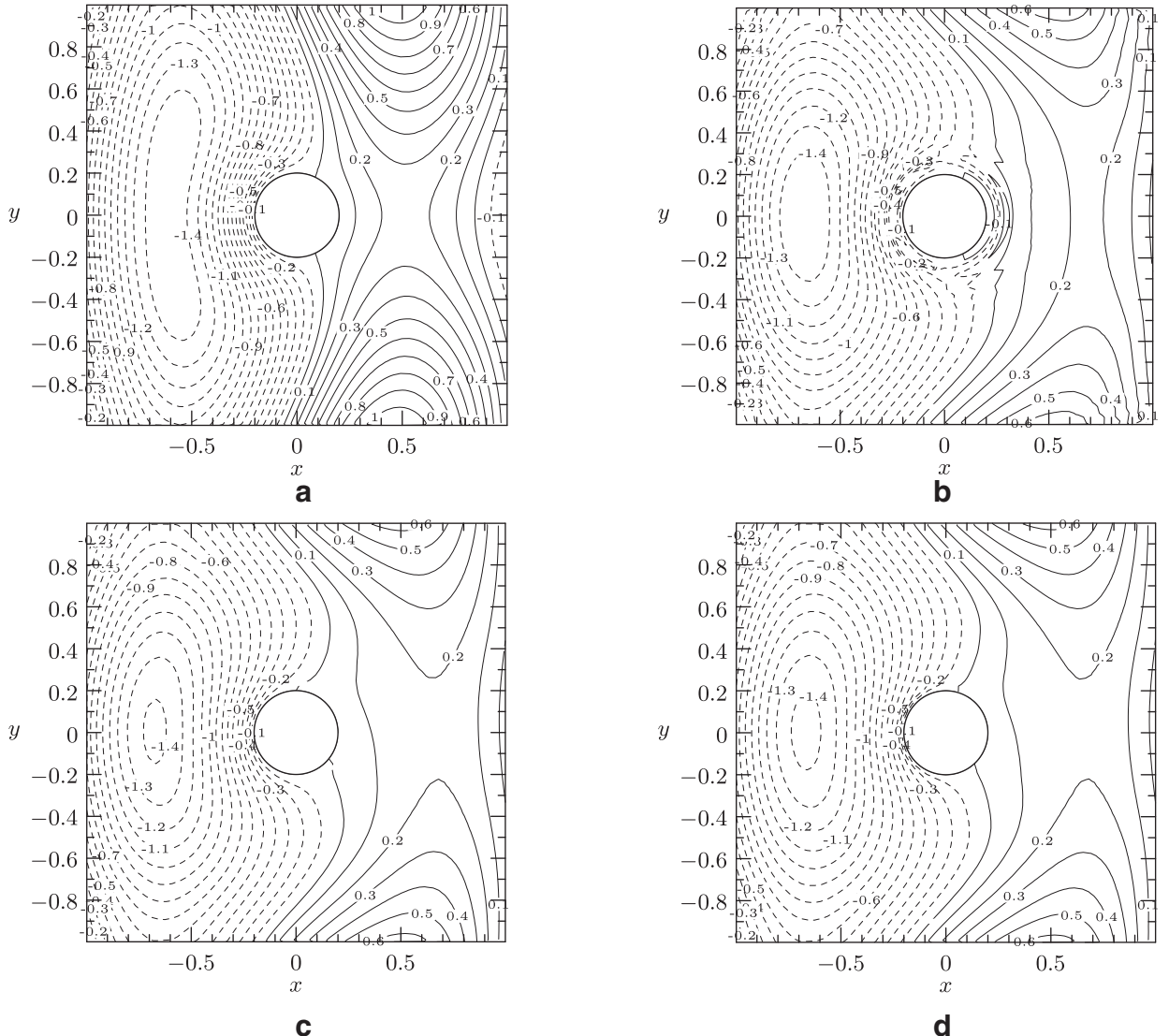


Fig. 25. (a) The exact analytical solution of E_z for 2D scattering problem at $t = 0.4$. The density plot of E_z at $t = 0.4$ for several RD schemes are given in (b) explicit Lax-Wendroff scheme, (c) RK2 LDA scheme after applying row-mass lumping, and (d) consistent mass-matrix time-backward LDA scheme.

$$\kappa_{mn}^2 = \kappa_m^2 + \kappa_n^2, \quad (6.13c)$$

$$\beta = \text{propagation coefficient} \rightarrow \omega^2 \mu \varepsilon - \beta^2 = \kappa_{mn}^2, \quad (6.13d)$$

and μ is the magnetic permeability, ε is the electric permittivity. The angular frequency is fixed at $\omega = 2\pi$, $E_0 = 1.0$, and $\mu = 1$, $\varepsilon = 1$ so that the speed of the waves is $c = 1/\sqrt{\mu\varepsilon} = 1$. In this study, only the lowest order mode of propagation will be considered, such that $m = n = 1$. Since the computational domain is $\{\Omega: 0 \leq x \leq 1, 0 \leq y \leq 1, 0 \leq z \leq 0.5\}$, a and b are the corresponding size of the waveguide in respective x and y -coordinates, therefore, $a = b = 1$. This set of data would be sufficient to calculate for the remaining propagation information κ_m , κ_n , κ_{mn} and β listed in Eq. (6.13). Apart from explicit Lax-Wendroff's, another two RD schemes tested are RD-Galerkin and RD-LDA schemes. For Lax-Wendroff and Galerkin schemes, both are made explicit simply by using the leapfrog time-discretization. On the other side, RD-LDA scheme is made explicit by RK2 time-discretization, as discussed in Section 5.5. Besides that, backward-time discretization for Galerkin and LDA schemes are also studied, both with the consistent mass-matrix and lumped mass-matrix. The reason of doing so although the explicit scheme is comfortably available is to observe how much the row-mass-lumping would baffle the order-of-accuracy.

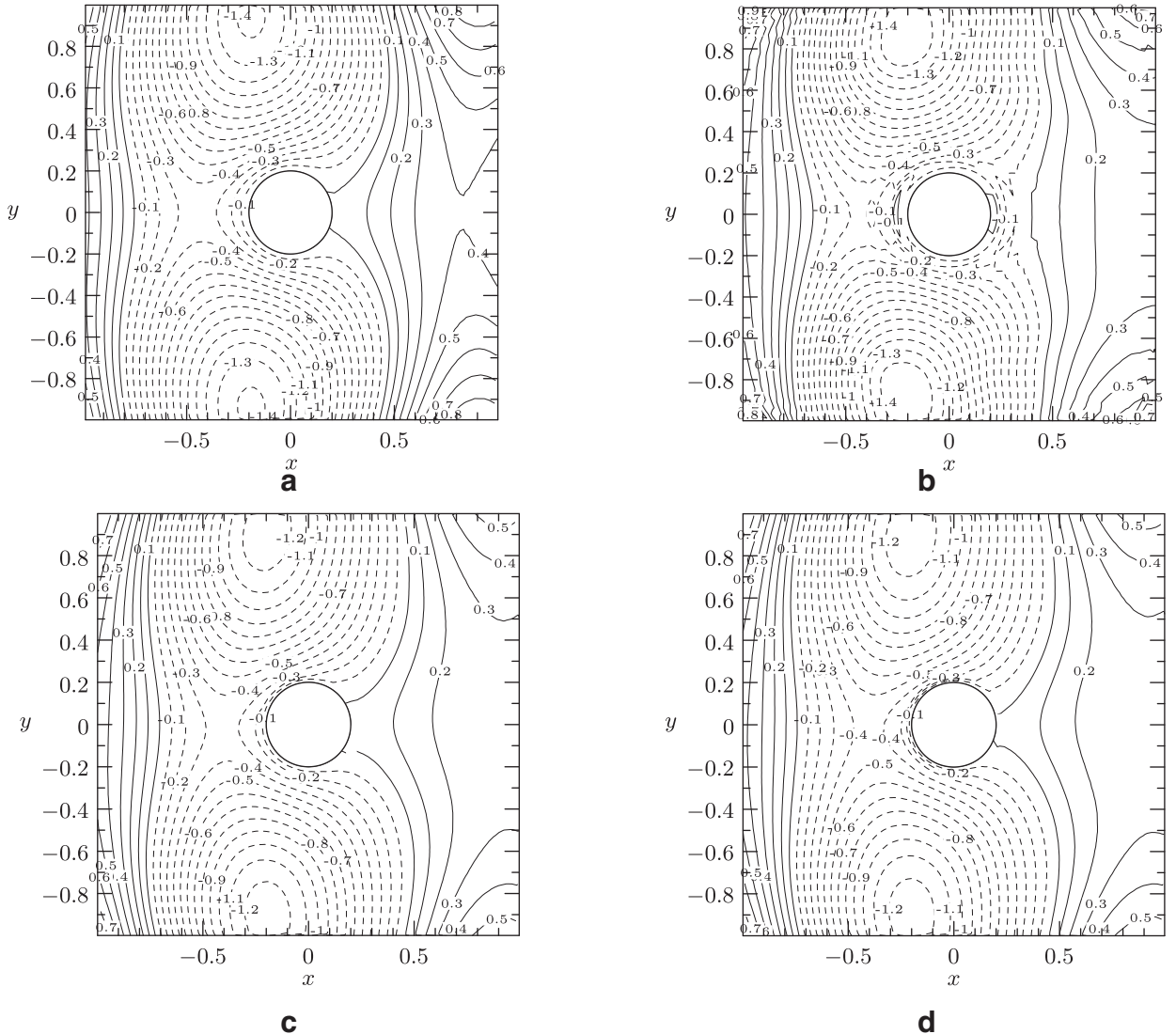


Fig. 26. (a) The exact analytical solution of E_z for 2D scattering problem at $t = 0.8$. The density plot of E_z at $t = 0.8$ using (b) explicit Lax-Wendroff scheme, (c) RK2 LDA scheme after applying row-mass lumping, and (d) consistent mass-matrix time-backward LDA scheme.

After all, the 3D plot might not be pellucid enough to study, as the components on the top have shrouded over the field-components stacking underneath. Thus, cross-sectional plots along $x = 0.5$ and at $z = 1$ are more ideal for viewing the wave patterns.

The tests were run from two aspects, the first one is to access the cross-sectional plots after long run on the coarsest grid to vitiate the numerical results more. The numerical results are then discernible after 100 time steps. The contour plots for lumped LDA scheme with RK2 time-stepping are given in Fig. 27 for cross-section x and Fig. 28 for cross-section z . In addition, further cross-sectional plots are also given in Figs. 29 and 30. All the cross-sectional plots are carried on the coarsest grids, which is $40 \times 40 \times 20$ for rectangular waveguide.

The second aspect is to prove the second-order-accuracy of the linear-preserving RD scheme. Three structured grids as shown in Fig. 31 with different mesh number were tested. The nodal update ceased after 20 time steps for each corresponding mesh to prevent the growing of global errors in time $O(\Delta t^2)$. Since the time step for each grid has to comply with the CFL condition, Δt is definitely smaller on finer grid $\Delta t = 0.000877193$ (mesh of $64 \times 64 \times 32$), and larger on coarser grid $\Delta t = 0.00172414$ (mesh of $40 \times 40 \times 20$), therefore the final time step t_f would be slightly different. However, this should not afflict too much inconsistencies in the order-of-accuracy check as it concerns with the spatial accuracy but not the temporal. The order-of-accuracy is taken to be the gradient from the L_2 -errors plot against the grid size Δx , as shown in Fig. 32a for rectangular waveguide. Do take notice that the plots are given in logarithmic scale and the L_2 -errors for each plot point are tabulated in Table 3. It is indisputable that Galerkin approach and the LW scheme proffer more accurate results than the

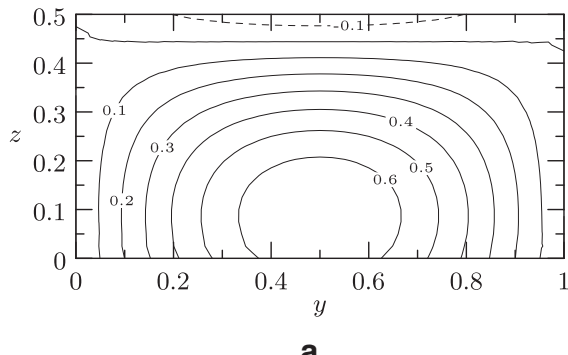
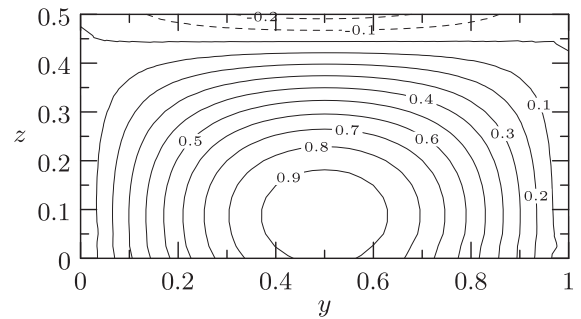
**a****b**

Fig. 27. The cross-sectional plots for $40 \times 40 \times 20$ rectangular waveguide at (a) $x = 0.25$, and (b) $x = 0.5$ after 100 time steps for lumped RD-LDA scheme with RK2 time-stepping.

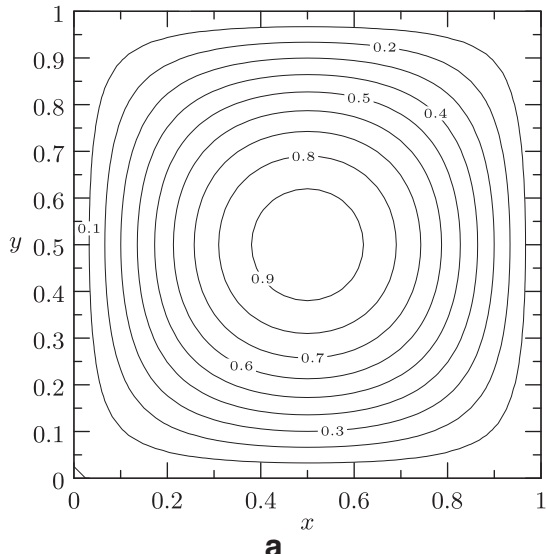
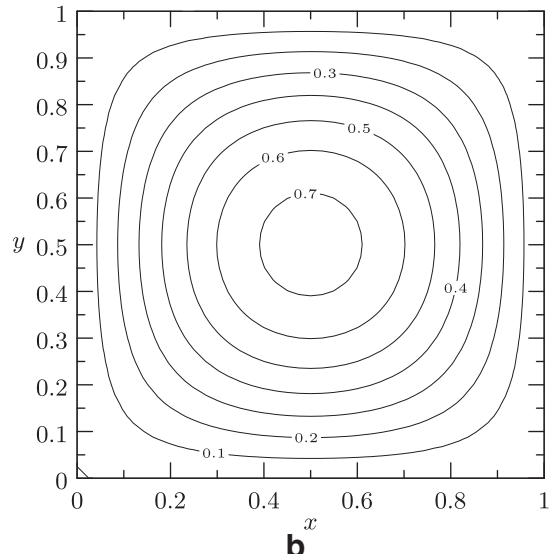
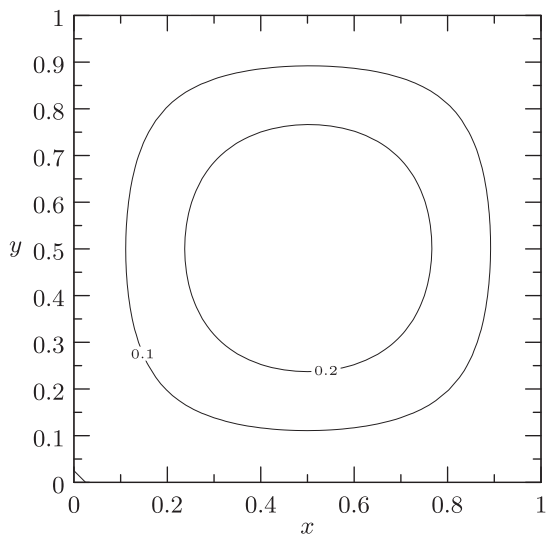
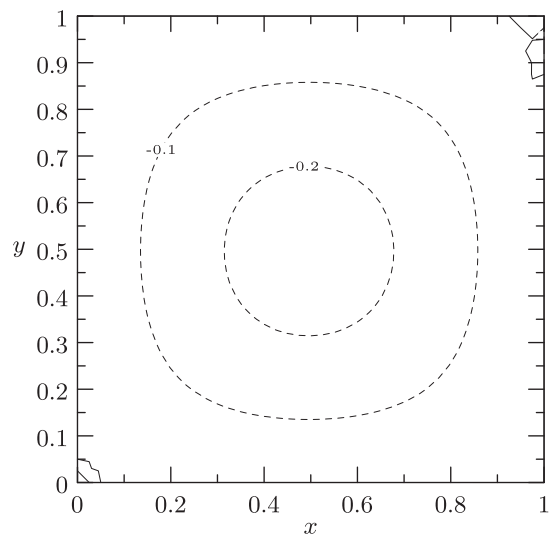
**a****b****c****d**

Fig. 28. The cross-sectional plots for $40 \times 40 \times 20$ rectangular waveguide at (a) $z = 0.125$, (b) $z = 0.25$, (c) $z = 0.375$ and (d) $z = 0.5$ after 100 time steps by lumping the LDA scheme and using the RK2 time-discretization.

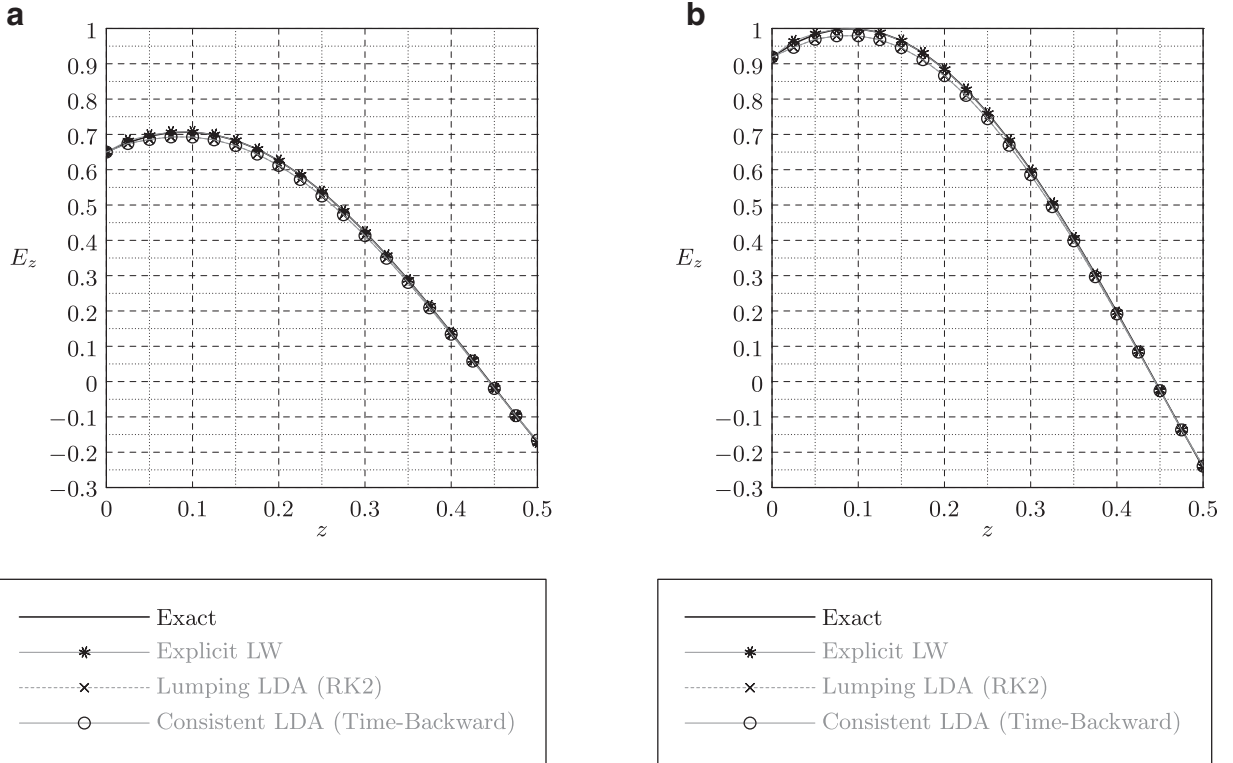


Fig. 29. The cross-sectional plots for $40 \times 40 \times 20$ rectangular waveguide at (a) $x = 0.25, y = 0.5$, and (b) $x = 0.5, y = 0.5$ after 100 time steps for RD-LW, lumping RD-LDA RK2 and consistent RD-LDA time-backward schemes.

Table 3

The gradient of the $\log L_2$ -errors against the $\log \Delta x$ gives the order-of-accuracy for RD scheme. The L_2 -errors are computed from $|E_z - \tilde{E}_z|$ after $20\Delta t$.

RD schemes	Rectangular waveguide
LW scheme	2.98595
Galerkin (Explicit leapfrog)	2.98339
Galerkin (Lumping backward-time)	2.97728
Galerkin (Consistent backward-time)	2.97601
LDA (Lumping RK2)	2.48817
LDA (Lumping backward-time)	2.36592
LDA (Consistent backward-time)	2.36228

upwind LDA scheme, due to the symmetrical distribution of their flux residual. In contrast, the upwind LDA scheme could be interpreted to resemble a one-sided distribution in finite-difference method. However, due to multidimensional upwind behavior, the LDA scheme is accomplished by distributing flux-residual of third-order-accurate $\Phi^T = O(\Delta x^3)$, therefore, the global errors captured after n -th iterations would still be slightly less than (Δx^2) rather of (Δx) in one-sided difference formula.

From the results of 3D rectangular waveguide, the time step under CFL condition is very small. This has imparted more attention to the study of spatial-order-accuracy with only little effect from the time-discretization. Fig. 32b shows a gross account of the computational time needed for different RD schemes. The computational time here starts after computing the distribution matrix, until the last time loop ceases. This is because for every set of mesh, the distribution matrix has to be calculated once only unless the permittivity or the permeability of the material changes with time. The cross-sectional plots for rectangular waveguide from Figs. 29 and 30 show that RD-LW scheme emulates upwind LDA scheme at capturing the wave profile in this 3D rectangular waveguide problem. Another important observation from the results is that the lumping still preserve the second-order of accuracy, although the magnitude of errors are still a bit larger compared with its consistent mass-matrix approach.

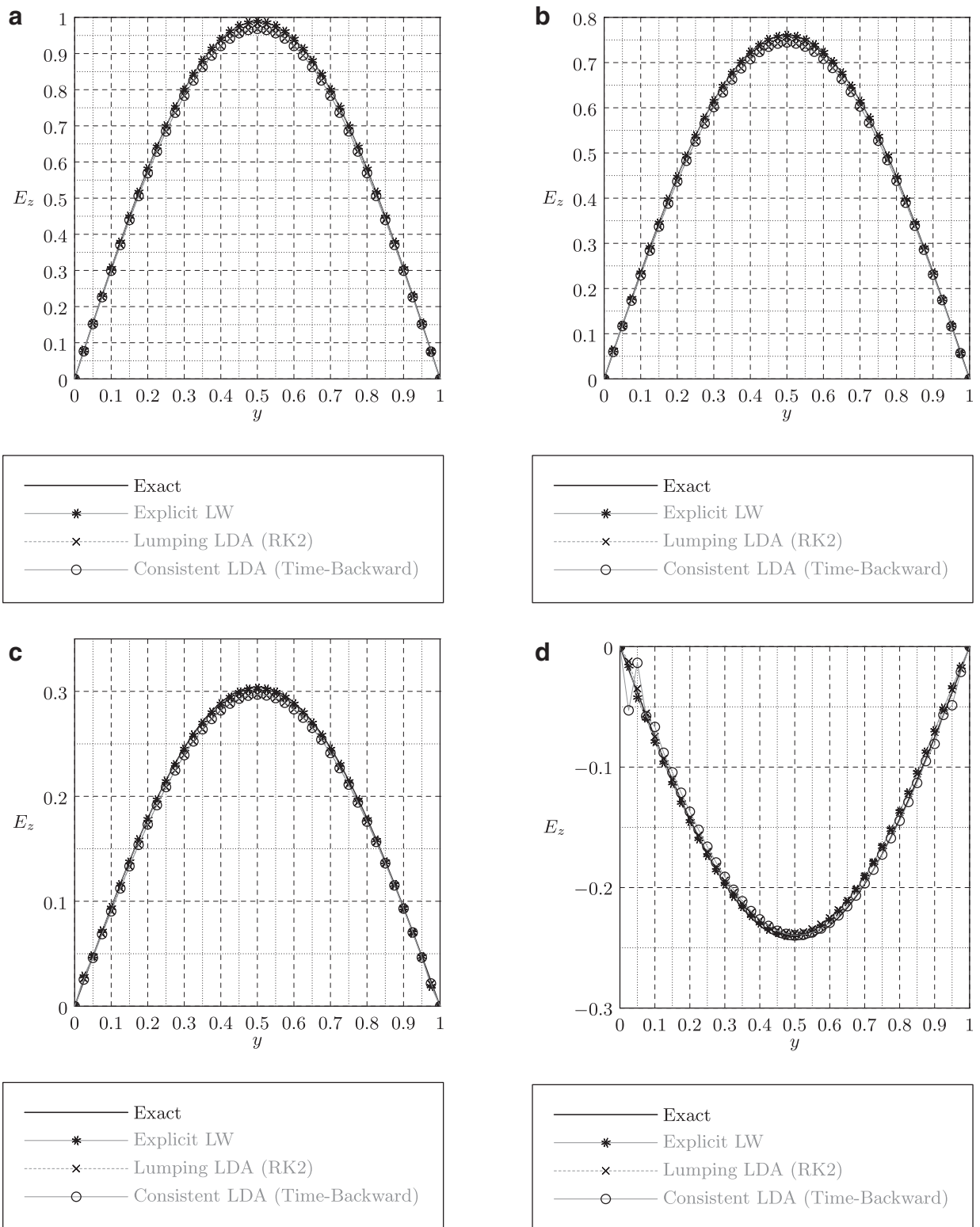


Fig. 30. The cross-sectional plots for $40 \times 40 \times 20$ rectangular waveguide at (a) $z = 0.125, x = 0.5$, (b) $z = 0.25, x = 0.5$, (c) $z = 0.375, x = 0.5$ and (d) $z = 0.5, x = 0.5$ after 100 time steps for a selected sample of RD schemes.

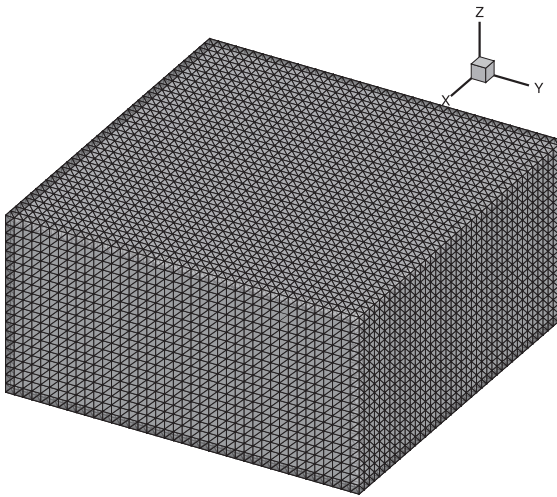


Fig. 31. The tetrahedral-structured mesh for rectangular waveguide.

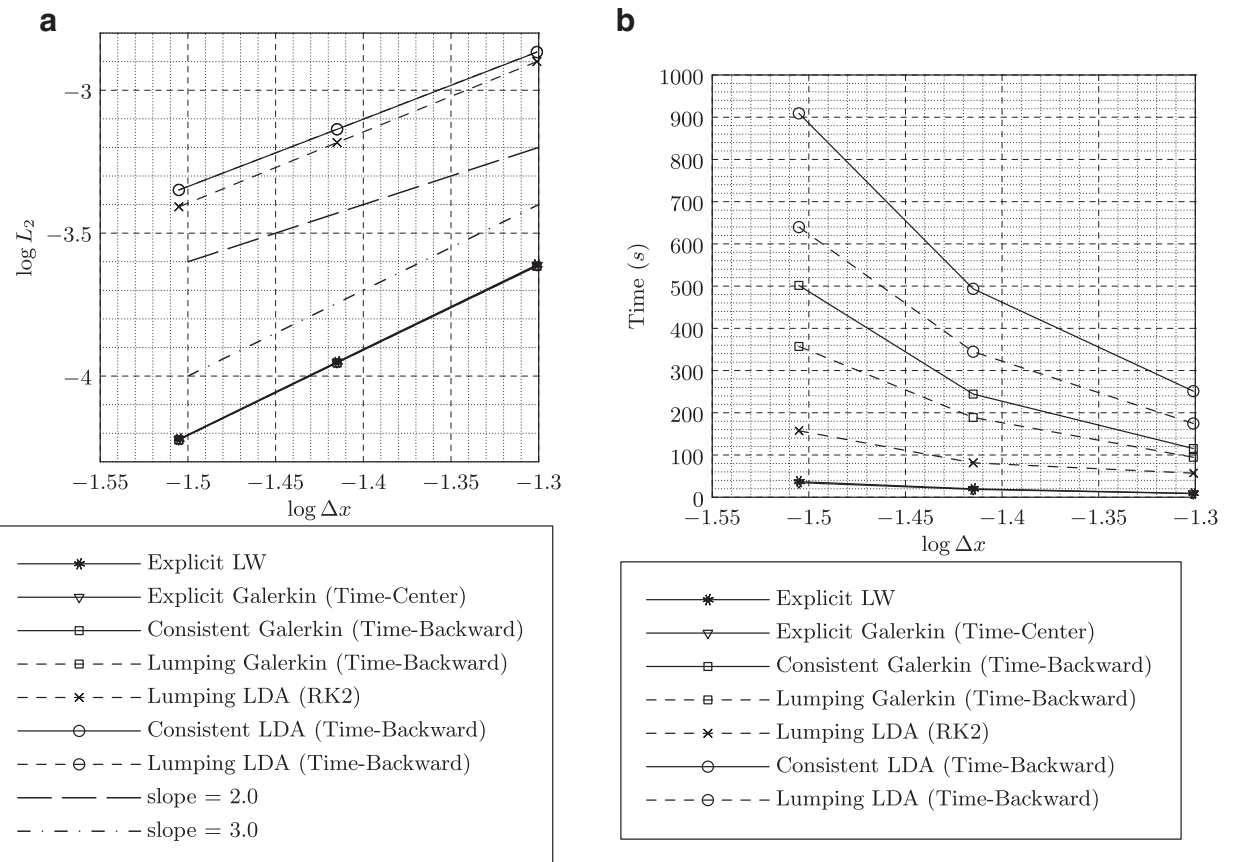


Fig. 32. (a) The L_2 -errors of several RD schemes superimposed in one single plot for 3D rectangular waveguide. The least-square gradient of each slope is given in Table 3. (b) The gross computational time of different RD schemes for rectangular waveguide.

Table 4

The CFL condition and pseudo-time step for waveguide test cases.

RD Scheme	2D Parallel-plate waveguide		3D rectangular waveguide	
	CFL	$\Delta\tau$	CFL	$\Delta\tau$
LW scheme	0.1	Irrelevant	0.8	Irrelevant
Galerkin (Explicit Leapfrog)	0.1	Irrelevant	0.8	Irrelevant
Galerkin (Lumping Backward-Time)	0.1	Δt	0.8	Δt^2
Galerkin (Consistent Backward-Time)	0.1	Δt	0.8	Δt^2
LDA (Explicit RK2)	0.1	Irrelevant	0.8	Irrelevant
LDA (Lumping Backward-Time)	0.1	$0.1\Delta t$	0.8	Δt^2
LDA (Consistent Backward-Time)	0.1	$0.1\Delta t$	0.8	Δt^2

Table 5

The CFL condition and pseudo-time step for 2D test cases involving radiation mechanism.

RD scheme	2D radiation		2D Hertzian-dipole		2D scattering	
	CFL	$\Delta\tau$	CFL	$\Delta\tau$	CFL	$\Delta\tau$
LW scheme	0.8	Irrelevant	0.5	Irrelevant	0.5	Irrelevant
LDA (Explicit RK2)	0.8	Irrelevant	0.3	Irrelevant	0.5	Irrelevant
LDA (Lumping backward-time)	0.8	$0.3\Delta t$	0.5	Δt^2	0.5	$0.08\Delta t$
LDA (Consistent backward-time)	0.8	$0.4\Delta t$	0.5	Δt^2	0.5	$0.08\Delta t$

For implicit schemes where the pseudo-time-stepping procedure is used, the stepping process ceases when the total residual for E_z is

$$\{\alpha_i^T(\mathbf{U}^{n+1,k+1}) + B_i^T \Phi^T(\mathbf{U}^{n+1,k+1})\} \leq 5 \times 10^{-7}. \quad (6.14)$$

It will take about 7–8 iterations to achieve this stopping criterion.

6.6. CFL condition and pseudo-time step

The CFL condition and pseudo-time step $\Delta\tau$ are the two fickle subjects in the computational process. Therefore, before closing up this section of results and discussions, Tables 4 and 5 are presented to give a forthright account on the choices of CFL number and $\Delta\tau$ for the order-of-accuracy test cases. As long as the CFL number is the same, the comparisons of different RD schemes on single test case would be fair even though $\Delta\tau$ might be different. This is because $\Delta\tau$ just plays the role of a scaling parameter that allows the solution to converge, and thus it can be any fraction of Δt . A full set of possible simulations was done on waveguide problem, namely the time-explicit, implicit lumping backward-time and implicit consistent backward-time. The explicit Galerkin is marched using leapfrog time-discretization whereas the explicit RK2 is employed for the LDA scheme. The RD-LW scheme is made explicit as described by Eqs. (4.8) and (4.10).

The attention of the authors is narrowed down to two schemes only for the 2D radiation and also the 2D scattering problems. The RD-Galerkin scheme is not presented here as it is deemed to behave in almost the same way as the LW scheme. The explicitly lumped LDA scheme with RK2 time-stepping is under the main consideration as it is the modification done by the authors.

7. Conclusions

The main purpose of this paper is to demonstrate on modifying for an explicit RD-LDA scheme, and to go against the concept that space-centered RD schemes are also suitable for solving certain time-dependent hyperbolic system, like the electromagnetic waveguide and radiation problems. The insistence by the authors to devise time-explicit scheme rather than complying with the time implicit RD-LDA scheme which is commonly found in RD framework is because time-explicit schemes are superior in term of computational cost. However, it is still avowed that implicit RD-LDA scheme preserves the order-of accuracy much better to its explicit counterpart after some long runs.

The RD scheme might be a propitious alternative for solving time-dependent Maxwell's equations. The compact stencil simplifies the nodal update procedure. For the explicit RD-LW and RD-Galerkin schemes, the order-of-accuracy is so well-preserved even with apparent explicit time-marching procedure, which actually comes from the mass-lumping procedure. The LDA scheme attests to its multidimensional-upwinding behaviour, when it comes to the scattering problem where the deformation with wave speed prevails. Another important remark about this LW scheme is that it collocates the time-derivative and flux divergence as $\partial/\partial t = -\mathcal{A} \cdot \nabla$, which might not be true if source exists. When the field components are discontinuous, or when an upwind scheme is inevitable, one might find the LDA scheme useful as it surpasses the usual drawback of one-sided upwind scheme being first-order accurate. In overall, the order-of accuracy for LDA scheme is about half an order lower than the Galerkin method or the LW scheme.

Acknowledgments

This work was partially supported by the Ministry of Higher Education MyBrain PhD Scholarship and Universiti Sains Malaysia Research University Grant-1001/PAERO/8014091. Besides, we would also like to express our utmost gratitude to all former or current members of our Computational Fluid Dynamics group, for their generosity during every discussion to share whatever they understood with us.

Appendix A. Consistent mass-matrix for upwind RD-scheme

In this appendix, several possible ways of constructing the mass-matrix are presented. The RD research community started to pay attention to the treatment of distributing the time-derivative, namely the unsteady residual when it comes to solving time-dependent problems using second-order-accurate solvers. All the matrices are presented as in its scalar form, where β_j is the distribution coefficient.

1. Streamline-upwind Petrov-Galerkin mass-matrix.

The first one, mostly ascribed to März and Degrez [34], using a similar technique as the stabilized finite-element method, whereby the mass-matrix is expressed as the well-known mass matrix of Petrov-Galerkin scheme.

$$\begin{aligned} m_{ij}^T &= \int_T \omega_i \psi_j d\Omega \\ &= \frac{S_T}{3} \begin{bmatrix} \beta_1^T + \frac{1}{6} & \beta_1^T - \frac{1}{12} & \beta_1^T - \frac{1}{12} \\ \beta_2^T + \frac{1}{12} & \beta_2^T - \frac{1}{6} & \beta_2^T - \frac{1}{12} \\ \beta_3^T + \frac{1}{12} & \beta_3^T - \frac{1}{12} & \beta_3^T - \frac{1}{6} \end{bmatrix} \\ &= \frac{S_T}{36} (3\delta_{ij} + 12\beta_i - 1). \end{aligned} \quad (\text{A.1})$$

2. Simple upwind mass-matrix of Caraeni.

Several years later, an idea conceived by Caraeni [11] that both the steady and unsteady residuals should be distributed based on β_i^T coefficients, such that his simple-upwind scheme reads

$$\begin{aligned} m_{ij}^T &= \frac{S_T}{3} \begin{bmatrix} \beta_1^T & \beta_1^T & \beta_1^T \\ \beta_2^T & \beta_2^T & \beta_2^T \\ \beta_3^T & \beta_3^T & \beta_3^T \end{bmatrix} \\ &= \frac{S_T}{3} \beta_i. \end{aligned} \quad (\text{A.2})$$

3. Hybrid-central-upwind mass-matrix.

Besides the already mentioned simple-upwind mass-matrix, Caraeni in his work [11] also proposed another way of constructing the mass-matrix, although it was professed that it didn't suit well for problems with discontinuities, which is rarely the case for Maxwell's equations

$$\begin{aligned} m_{ij}^T &= \frac{S_T}{36} \begin{bmatrix} 22\beta_1^T & 7\beta_1^T & 7\beta_1^T \\ 7\beta_2^T & 22\beta_2^T & 7\beta_2^T \\ 7\beta_3^T & 7\beta_3^T & 22\beta_3^T \end{bmatrix} \\ &= S_T \gamma_{ij} \beta_i, \end{aligned} \quad (\text{A.3})$$

where

$$\gamma_{ij} = \begin{cases} \frac{22}{36} & \text{for } i = j \\ \frac{7}{36} & \text{for } i \neq j. \end{cases} \quad (\text{A.4})$$

4. Consistent-upwind mass-matrix (de Palma and et al.).

De Palma [16] and his colleagues have presented another exquisite way of constructing the consistent-upwind mass-matrix, by carefully suggesting that there might be infinite way of constructing consistent mass-matrix as long as the distribution of the unsteady residual is conservative.

$$\begin{aligned} m_{ij}^T &= \frac{S_T}{3} \begin{bmatrix} \beta_1^T(2 - \beta_1^T) & \beta_1^T(1 - \beta_2^T) & \beta_1^T(1 - \beta_3^T) \\ \beta_2^T(1 - \beta_1^T) & \beta_2^T(2 - \beta_2^T) & \beta_2^T(1 - \beta_3^T) \\ \beta_3^T(1 - \beta_1^T) & \beta_3^T(1 - \beta_2^T) & \beta_3^T(2 - \beta_3^T) \end{bmatrix} \\ &= \frac{S_T}{3} \beta_i (\delta_{ij} + 1 - \beta_j^T). \end{aligned} \quad (\text{A.5})$$

5. *Consistent-upwind mass-matrix (Ricchiuto and Abgrall).*

Ricchiuto and Abgrall [44] when developing their high-order mass-lumping approach to obtain an explicit time-marching for upwind scheme, hence also derived another member to the family of consistent mass-matrix that reads

$$\begin{aligned} m_{ij}^T &= \frac{S_T}{3} \begin{bmatrix} (\beta_1^T)^2 & \beta_1^T(1+\beta_2^T) & \beta_1^T(1+\beta_3^T) \\ \beta_2^T(1+\beta_1^T) & (\beta_2^T)^2 & \beta_2^T(1+\beta_3^T) \\ \beta_3^T(1+\beta_1^T) & \beta_3^T(1+\beta_2^T) & (\beta_3^T)^2 \end{bmatrix} \\ &= \frac{S_T}{3} \beta_i(1 - \delta_{ij} + \beta_j^T). \end{aligned} \quad (\text{A.6})$$

The full derivation of these consistent mass-matrices could be found in [16,48] or the very complementary work from Ricchiuto and Abgrall [44] which incorporated the idea of high-order mass-lumping into RD framework.

Appendix B. Derivation of RD-Lax-Wendroff scheme (Weak formulation)

Rossiello and his collaborators [50] have provided some very clear derivations of LW from weak formulation perspective, which would only be summarized here. From their discussions, it is not difficult to figure out that the LW is made explicit by lumping, which is not shown if one views it from the control-volume approach given in Section 4.2

$$\begin{aligned} &\sum_{T \in \cup \Delta_i} \iint_T \psi_i I \left(\frac{\partial \mathbf{U}_h}{\partial t} + \nabla \cdot \mathcal{F}_h(\mathbf{U}) \right)^{n+\frac{1}{2}} d\Omega \\ &= \underbrace{\sum_{T \in \cup \Delta_i} \iint_T \psi_i I \sum_{j \in T} \psi_j^T \frac{\Delta \mathbf{U}_j}{\Delta t} d\Omega}_{A} + \underbrace{\sum_{T \in \cup \Delta_i} \iint_T \psi_i I (\nabla \cdot \bar{\mathbf{F}}_h(\mathbf{U}))^{n+\frac{1}{2}} d\Omega}_{B}. \end{aligned} \quad (\text{B.1})$$

The first term of Eq. (B.1) could be discretized as

$$\begin{aligned} A &= \sum_{T \in \cup \Delta_i} \iint_T \psi_i I \sum_{j \in T} \psi_j^T \left(\frac{\mathbf{U}_j^{n+1} - \mathbf{U}_j^n}{\Delta t} \right) d\Omega \\ &\approx S_i \frac{\mathbf{U}_i^{n+1} - \mathbf{U}_i^n}{\Delta t}. \end{aligned} \quad (\text{B.2a})$$

The last expression of Eq. (B.2a) can only be arrived by assuming that integration of the product of two Lagrange's interpolating functions gives back one-third of the element area

$$\iint_T \psi_i I \psi_j d\Omega = \frac{S_T}{3}. \quad (\text{B.2b})$$

The second term of Eq. (B.1) is manipulated after the substitution of relation given by Eq. (4.7),

$$\begin{aligned} B &= \sum_{T \in \cup \Delta_i} \iint_T \psi_i I \left(\frac{\partial \mathcal{F}_h}{\partial t} \cdot \nabla \mathbf{U}_i \right)^{n+\frac{1}{2}} d\Omega \\ &= - \sum_{T \in \cup \Delta_i} \iint_T \psi_i I \left(\frac{\partial \mathbf{U}_i}{\partial t} \right)^n d\Omega - \sum_{T \in \cup \Delta_i} \frac{\Delta t}{2} \iint_T \psi_i I \left(\frac{\partial^2 \mathbf{U}_i}{\partial t^2} \right)^n d\Omega + O(\Delta t^2) \\ &= \sum_{T \in \cup \Delta_i} \left\{ \iint_T \psi_i I (\mathcal{A} \cdot \nabla \mathbf{U})^n d\Omega - \frac{\Delta t}{2} \iint_T \psi_i I [\mathcal{A} \cdot \nabla (\mathcal{A} \cdot \nabla \mathbf{U})]^n d\Omega + O(\Delta t^2) \right\} \\ &= \sum_{T \in \cup \Delta_i} \left\{ \iint_T \psi_i I (\mathcal{A} \cdot \nabla \mathbf{U})^n d\Omega - \frac{\Delta t}{2} \iint_T \nabla \cdot [\mathcal{A} \cdot \nabla (\mathcal{A} \cdot \nabla \mathbf{U})^n \psi_i I \mathcal{A}] d\Omega \right. \\ &\quad \left. - \frac{\Delta t}{2} \iint_T (\mathcal{A} \cdot \nabla \mathbf{U})^n [\nabla \cdot (\psi_i I \mathcal{A})] d\Omega \right\} + O(\Delta t^2) \\ &= \sum_{T \in \cup \Delta_i} \left\{ \iint_T S_T \frac{I}{3} (\mathcal{A} \cdot \nabla \mathbf{U})^n - \frac{\Delta t}{2} \oint_{\partial T} [(\mathcal{A} \cdot \nabla \mathbf{U})^n \psi_i I \mathcal{A}] \cdot d\hat{\ell} \right. \\ &\quad \left. + \frac{\Delta t}{2} (\mathcal{A} \cdot \nabla \mathbf{U})^n \iint_T [\nabla \cdot (\psi_i I \mathcal{A})] d\Omega \right\} + O(\Delta t^2), \end{aligned} \quad (\text{B.2c})$$

where I is the identity matrix, and the following vector identity has been used

$$\nabla \cdot (b\mathbf{A}) = \mathbf{A} \cdot \nabla b + b(\nabla \cdot \mathbf{A}), \quad (\text{B.3})$$

by letting

$$\mathbf{A} = \psi_i I \mathcal{A}, \quad b = \mathcal{A} \cdot \nabla \mathbf{U}. \quad (\text{B.4})$$

The second term of Eq. (B.2c) is equal to zero when sum over set of elements sharing node i as their contributions from the internal edges eliminate one another. Thus, Eq. (B.2c) reduces to

$$B = \sum_{T \in \cup \Delta_i} \left\{ \frac{I}{3} \sum_{j \in T} \frac{\mathcal{A} \cdot \mathbf{n}_j}{2} \mathbf{U} + \frac{\Delta t}{2} \frac{\mathcal{A} \cdot \mathbf{n}_j}{2S_T} \sum_{j \in T} \frac{\mathcal{A} \cdot \mathbf{n}_j}{2} \right\}, \quad (\text{B.5})$$

as

$$(\mathcal{A} \cdot \nabla \mathbf{U})^n = \sum_{j \in T} \frac{\mathcal{A} \cdot \mathbf{n}_j}{2S_T} \mathbf{U}_j = \frac{\Phi^T}{S_T}.$$

The substitution of Eqs. (B.2) back into (B.1) gives the RD-LW approach

$$\mathbf{U}_i^{n+1} = \mathbf{U}_i^n - \frac{\Delta t}{S_i} \sum_{T \in \cup \Delta_i} \left[\frac{1}{3} I + \frac{\Delta t}{2S_T} K_i^T \right] \Phi_j^T, \quad (\text{B.6a})$$

with the distribution matrix B_j^{LW} given as

$$B_j^T = \frac{1}{3} I + \frac{\Delta t}{2S_T} K_j^T. \quad (\text{B.6b})$$

References

- [1] R. Abgrall, Toward the ultimate conservative scheme : following the quest, *J. Comput. Phys.* 167 (2001) 277–315.
- [2] R. Abgrall, Residual distribution schemes : current status and future trends, *Comput. Fluids* 35 (2006) 641–669.
- [3] R. Abgrall, P. Bacigaluppi, S. Tokareva, High-order residual distribution scheme for the time-dependent euler equations of fluid dynamics, *Comput. Math. Appl.*, in press.
- [4] R. Abgrall, R. Huart, P. Ramet, Numerical simulation of unsteady MHD flows and applications, *Magnetohydrodynamics* 45 (2) (2009) 225–232.
- [5] N. Aslan, Mhd-a : a fluctuation splitting wave model for planar magnetohydrodynamics, *J. Comput. Phys.* 153 (1999) 437–466.
- [6] C.A. Balanis, Advanced engineering electromagnetics, 1st, John-Wiley & Sons, 1989.
- [7] H.S. Bhat, B. Osting, Kirchoff's laws as a finite volume method for the planar Maxwell equations, *IEEE Trans. Antennas Propag.* 59 (10) (2011) 3772–3779.
- [8] B. Bidégaray, J.-M. Ghidaglia, Multidimensional corrections to cell-centered finite volume methods for Maxwell equations, *Appl. Numer. Math.* 44 (2003) 281–298.
- [9] A. Bondeson, T. Rylander, P. Ingelström, Computational Electromagnetics, Springer Science+Business Media, 2005.
- [10] P. Bonnet, X. Ferrières, B. Michelsen, P. Klotz, Time Domain Electromagnetics, Academic Press, pp. 307–367.
- [11] D.A. Caraeni, Development of a multidimensional residual distribution solver for large Eddy simulation of industrial turbulent flows, Lund Institute of Technology, 2000 Ph.D. Thesis.
- [12] C. Christopoulos, The Transmission-Line Modeling Method (TLM), IEEE Press, Piscataway, NJ, 1995.
- [13] C. Christopoulos, The Transmission-Line Modeling (TLM) Method in Electromagnetics, Morgan & Claypool, San Rafael, CA, 2006.
- [14] J.P. Cioni, L. Fézoui, D. Issautier, High-order upwind schemes for solving time-domain maxwell equations, *La Recherche Aérospatiale* 5 (1994) 319–328.
- [15] A.G. Csik, Upwind residual distribution schemes for general hyperbolic conservation laws and application to ideal magnetohydrodynamics, Katholieke Universiteit Leuven, 2002 Ph.D. thesis.
- [16] P. De Palma, G. Pascazio, G. Rossiello, M. Napolitano, A second-order-accurate monotone implicit fluctuation splitting scheme for unsteady problems, *J. Comput. Phys.* 208 (2005) 1–33.
- [17] H. Deconinck, H. Paillère, R. Struijs, P.L. Roe, Multidimensional upwind schemes based on fluctuation-splitting for system of conservation laws, *Comput. Mech.* 11 (1993a) 323–340.
- [18] H. Deconinck, M. Ricchiuto, Residual distribution schemes: foundations and analysis, in: E. Stein, R. de Borst, T. Hughes (Eds.), Encyclopedia of Computational Mechanics, John Wiley & Sons, Ltd., 2007.
- [19] H. Deconinck, M. Ricchiuto, K. Sermeus, Introduction to residual distribution schemes and comparison with stabilized finite elements, in: VKI LS 2003-05, 33rd Computational Fluid Dynamics Course, von Kármán Institute for Fluid Dynamics, 2003.
- [20] H. Deconinck, P.L. Roe, S. R., A multidimensional generalisation of Roe's flux difference splitter for the euler equations, *Comput. Fluids* 22 (2/3) (1993b) 2015–2222.
- [21] N. Deore, A. Chatterjee, A cell-vertex finite volume time domain method for electromagnetic scattering, *Progr. Electromagn. Res. M* 12 (2010) 1–15.
- [22] C. Fumeaux, D. Baumann, P. Bonnet, R. Vahldieck, Developments of finite-volume techniques for electromagnetic modeling in unstructured meshes, in: Proceedings of the 17th International Zurich Symposium on Electromagnetic Compatibility, 2006.
- [23] W.H.J. Hayt, J.A. Buck, Engineering Electromagnetics, 8th edition, McGraw Hill, 2012.
- [24] F. Hermeline, Two coupled particle-finite volume methods using Delaunay-Voronoi meshes for the approximation of Vlasov-Poisson and Vlasov-Maxwell equations, *J. Comput. Phys.* 106 (1993) 1–18.
- [25] W.J.R. Hoefer, The transmission-line matrix method – theory and applications, *IEEE Trans. Microw. Theory Tech.* 33 (1985) 882–893.
- [26] M.E. Hubbard, Non-oscillatory third order fluctuation splitting schemes for steady scalar conservation laws, *J. Comput. Phys.* 222 (2007) 740–768.
- [27] T.J.R. Hughes, The Finite Element Method - Linear Static and Dynamic Finite Element Analysis, Prentice-Hall Inc, Englewood Cliffs, 1987.
- [28] T.Z. Ismagilov, Second order finite volume scheme for Maxwell's equations with discontinuous electromagnetic properties on unstructured meshes, *J. Comput. Phys.* 282 (2015) 33–42.
- [29] F. Ismail, H. Chizari, Developments of entropy-stable residual distribution methods for conservation laws i : scalar problems, *J. Comput. Phys.* 330 (2017) 1093–1115.
- [30] A. Jameson, Time-dependent calculations using multigrid, with applications to unsteady flow past airfoils and wings, in: Proceedings of the AIAA 10th Computational Fluid Dynamics Conference, 1991.

- [31] L. Koloszár, N. Villedieu, T. Quintino, P. Rambaud, H. Deconinck, J. Anthoine, Residual distribution method for aeroacoustics, *AIAA J.* 49 (5) (2011).
- [32] N.K. Madsen, R.W. Ziolkowski, Numerical solution of Maxwell's equations in the time domain using irregular nonorthogonal grids, *Wave Motion* 10 (6) (1988) 583–596.
- [33] N.K. Madsen, R.W. Ziolkowski, A three-dimensional modified finite volume technique for Maxwell's equations, *Electromagnetics* 10 (1) (1990) 147–161.
- [34] J. März, G. Degrez, Improving time accuracy for residual distribution schemes., Technical Report, VKI-DC report 1996-17, 1996.
- [35] A. Mazaheri, H. Nishikawa, Improved second-order hyperbolic residual-distribution scheme and its extension to third-order on arbitrary triangular grids, *J. Comput. Phys.* 300 (2015) 455–491.
- [36] N.Z. Mebrane, High order fluctuation splitting schemes for hyperbolic conservation laws, School of Computing, The University of Leeds, 2007 Ph.D. thesis.
- [37] R.-H. Ni, A multiple grid scheme for solving the euler equations, *Am. Inst. Aeronaut. Astronaut.* 20 (1981) 1565–1571.
- [38] H. Paillière, Multidimensional upwind residual discretization scheme for the Euler and Navier-Stokes equations on unstructured meshes, Université Libre de Bruxelles, 1995 Ph.D. thesis.
- [39] S. Piperno, M. Remaki, L. Fezoui, A nondiffusive finite volume scheme for the three-dimensional Maxwell's equations on unstructured meshes, *SIAM J. Numer. Anal.* 39 (6) (2002) 2089–2108.
- [40] Z. Popović, B.D. Popović, Introductory Electromagnetics, Prentice-Hall, 2000.
- [41] D.M. Pozar, Microwave Engineering, fourth, John-Wiley & Sons, 2012.
- [42] J.N. Reddy, An Introduction to the Finite Element Method, Second edition, McGraw-Hill Inc, 1993.
- [43] M. Remaki, A new finite volume scheme for solving Maxwell system, *COMPEL - The Int. J. Comput. Math. Electr. Electr. Eng.* 19 (3) (2000) 913–932.
- [44] M. Ricchiuto, R. Abgrall, Explicit Runge-Kutta residual distribution schemes for time dependent problems : second order case, *J. Comput. Phys.* 229 (2010) 5653–5691.
- [45] P.L. Roe, Approximate Riemann solvers, parameter vectors, and difference schemes, *J. Comput. Phys.* 43 (1981) 357–372.
- [46] P.L. Roe, Fluctuation and signals - a framework for numerical evolution problems, in: K.W. Morton, M.J. Baines (Eds.), *Numerical Methods for Fluid Dynamics*, Academic Press, 1982, pp. 219–257.
- [47] P.L. Roe, Linear advection schemes on triangular meshes, CoA Report, Cranfield Institute of Technology, 1987.
- [48] Rossiello, High-order accurate residual distribution methods for unsteady compressible flow, Politecnico di Bari, 2004 Ph.D. thesis.
- [49] G. Rossiello, P. De Palma, G. Pascazio, M. Napolitano, Analysis of high-order-accurate fluctuation splitting schemes for steady advection, *Int. J. Comput. Fluid Dynamics* 24 (6) (2010) 217–225.
- [50] G. Rossiello, P. de Palma, G. Pascazio, M. Napolitano, Second-order-accurate explicit fluctuation splitting schemes for unsteady problems, *Comput. Fluids* 38 (2009) 1384–1393.
- [51] J.A. Rossmanith, A class of residual distribution schemes and their relation to relaxation systems, *J. Comput. Phys.* 227 (22) (2008) 9527–9553.
- [52] M. Rudgyard, Cell-vertex methods for steady inviscid flow, VKI lecture series 1993-04, Computational Fluid Dynamics, 1993.
- [53] M.N.O. Sadiku, *Numerical Techniques in Electromagnetics*, Second edition, CRC Press LLC, 2001.
- [54] V. Shankar, F.W. Hall, A.H. Mohammadian, A time-domain differential solver for electromagnetic scattering problems, *Proc. IEEE* 77 (5) (1989) 709–721.
- [55] V. Shankar, A.H. Mohammadian, W.F. Hall, A time-domain, finite-volume treatment for the Maxwell equations, *Electromagnetics* 10 (1–2) (1990) 127–145.
- [56] D. Sidilkover, Numerical solution to steady-state problems with discontinuities, Wiesmann Institute, Israel, 1990 Ph.D. thesis.
- [57] D. Sidilkover, P.L. Roe, Unifications of some advection schemes in two dimensions, Technical Report, Institute for Computer Applications in Science and Engineering (ICASE), NASA Langley Research Center, 1995.
- [58] J.L. Steger, R.F. Warming, Flux vector splitting of the inviscid gasdynamic equations with application to finite-difference methods, *J. Comput.* 40 (1981) 263–293.
- [59] R. Struijs, H. Deconinck, P. de Palma, P.L. Roe, K.G. Powell, Progress on multidimensional upwind euler solvers for unstructured grids, *Am. Inst. Aeronaut. Astronaut.* 91 (1550) (1991a).
- [60] R. Struijs, H. Deconinck, P.L. Roe, Fluctuation splitting schemes for the 2d euler equations., VKI lecture series 1991-01, Computational Fluid Dynamics, 1991b.
- [61] A. Taflove, *Computational Electrodynamics : The Finite-Difference Time-Domain Method*, Artech House, Norwood, MA, 1995.
- [62] F.T. Ulaby, E. Michielssen, U. Ravaioli, *Fundamentals of Applied Electrodynamics*, 6th, Prentice-Hall, 1994.
- [63] A. Warzyński, M.E. Hubbard, M. Ricchiuto, Runge-Kutta residual distribution schemes, *J. Sci. Comput.* 62 (3) (2015) 772–802.
- [64] K.S. Yee, Numerical solution of initial boundary value problems involving Maxwell's equations in isotropic media, *IEEE Trans. Antennas Propag.* 14 (3) (1966) 302–307.
- [65] K.S. Yee, J.S. Chen, Conformal finite difference time domain and finite volume time domain, *IEEE Trans. Antennas Propag.* 42 (10) (1994) 1450–1455.
- [66] K.S. Yee, J.S. Chen, Impedance boundary condition simulation in the FDTD/FVTD hybrid, *IEEE Trans. Antennas Propag.* 45 (6) (1997) 921–925.